Mineralogy and Petrology

The tetrad effect and geochemistry of apatite from the Altay Koktokay No. 3 pegmatite, Xinjiang, China: Implications for pegmatite petrogenesis

--Manuscript Draft--

Manuscript Number:	MIPE402R2
Full Title:	The tetrad effect and geochemistry of apatite from the Altay Koktokay No. 3 pegmatite, Xinjiang, China: Implications for pegmatite petrogenesis
Article Type:	Standard Article
Keywords:	Tetrad effect; Y/Ho ratio; apatite; Koktokay No. 3 pegmatite
Corresponding Author:	Mingjian Cao, Ph.D. Institute of Geology and Geophysics, Chinese Academy of Sciences Beijing, Beijing CHINA
Corresponding Author Secondary Information:	
Corresponding Author's Institution:	Institute of Geology and Geophysics, Chinese Academy of Sciences
Corresponding Author's Secondary Institution:	
First Author:	Mingjian Cao, Ph.D.
First Author Secondary Information:	
Order of Authors:	Mingjian Cao, Ph.D.
	Qifeng Zhou, Dr.
	Kezhang Qin, Dr.
	Dongmei Tang, Dr.
	Noreen J. Evans, Dr.
Order of Authors Secondary Information:	
Abstract:	In order to better constrain the evolution and petrogenesis of pegmatite, geochemical analysis was conducted on a suite of apatite crystals from the Altay Koktokay No. 3 pegmatite, Xinjiang, China and from the granitic and amphibolitic wall rocks. Apatite samples derived from pegmatite zones show convex tetrad effects in their REE patterns, extremely negative Eu anomalies and non-chondritic Y/Ho ratios. In contrast, chondritic Y/Ho ratios and convex tetrad effects are observed in the muscovite granite suggesting that different processes caused non-chondritic Y/Ho ratios and lanthanide tetrad effects. Based on the occurrence of convex tetrad effects in the host rocks and their associated minerals, we propose that the tetrad effects are likely produced from immiscible fluoride and silicate melts. This is in contrast to previous explanations of the tetrad effect; i.e. surface weathering, fractional crystallization and/or fluid-rock interaction. Additionally, we put forward that extreme negative Eu and non-chondritic Y/Ho in apatite are likely caused by the large amount of hydrothermal fluid exsolved from the pegmatite melts. Evolution of melt composition was found to be the primary cause of inter and intra-crystal major and trace element variations in apatite. Mn entering into apatite via substitution of Ca is supported by the positive correlation between CaO and MnO. Different evolution trends in apatite composition imply different crystallization environments between wall rocks and pegmatite zones. Based on the geochemistry of apatite samples, it is likely that there is a genetic relationship between the source of muscovite granite and the source of the pegmatite.
Response to Reviewers:	Firstly, we carefully read the editor's suggestions and revised this manuscript according to these suggestions. Secondly, the English native speaker Noreen J. Evans (one of our co-authors) have also carefully checked and edited this manuscript. The second revision on this corrected manuscript is marked with blue color, the text

	also shown the first revised parts with the read color.

The tetrad effect and geochemistry of apatite from the Altay Koktokay No. 3 pegmatite, Xinjiang, China: Implications for pegmatite petrogenesis

Ming-Jian Cao[1,2], Qi-Feng, Zhou[1,2], Ke-Zhang Qin[1], Dong-Mei Tang[1], Noreen J. Evans[3]

[1]Key Laboratory of Mineral Resources, Institute of Geology and Geophysics, Chinese Academy of Sciences, P.O. Box 9825, Beijing 100029, China

[2] Graduate University of Chinese Academy of Sciences, Beijing 100049, China

[3]CSIRO Earth Science and Resource Engineering, 26 Dick Perry Ave., Kensington, WA 6151, Australia and John de Laeter Center for Isotope Research, Dept. Applied Geology, Curtin University, Perth WA 6945, Australia and Department of Earth & Oceanic Sciences, The University of Waikato, Private Bag 3105, Hamilton New Zealand

Corresponding author:
Key Laboratory of Mineral Resources, Institute of Geology and Geophysics, Chinese Academy of Sciences, P.O. Box 9825, Beijing 100029, China. Phone: +86-10-82998183; Fax: +86-10-62010846; Email: kzq@mail.iggcas.ac.cn
Key Laboratory of Mineral Resources, Institute of Geology and Geophysics, Chinese Academy of Sciences, P.O. Box 9825, Beijing 100029, China. Phone: +86-10-82998190; Fax: +86-10-62010846; Email: caomingjian@mail.iggcas.ac.cn

Abstract

In order to better constrain the evolution and petrogenesis of pegmatite, geochemical analysis was conducted on a suite of apatite crystals from the Altay Koktokay No. 3 pegmatite, Xinjiang, China and from the granitic and amphibolitic wall rocks. Apatite samples derived from pegmatite zones show convex tetrad effects in their REE patterns, extremely negative Eu anomalies and non-chondritic Y/Ho ratios. In contrast, chondritic Y/Ho ratios and convex tetrad effects are observed in the muscovite granite suggesting that different processes caused non-chondritic Y/Ho ratios and lanthanide tetrad effects. Based on the occurrence of convex tetrad effects in the host rocks and their associated minerals, we propose that the tetrad effects are likely produced from immiscible fluoride and silicate melts. This is in contrast to previous explanations of the tetrad effect; i.e. surface weathering, fractional crystallization and/or fluid-rock interaction. Additionally, we put forward that extreme negative Eu and non-chondritic Y/Ho in apatite are likely caused by the large amount of hydrothermal fluid exsolved from the pegmatite melts.

Evolution of melt composition was found to be the primary cause of inter and intra-crystal major and trace element variations in apatite. Mn entering into apatite via substitution of Ca is supported by the positive correlation between CaO and MnO. Different evolution trends in apatite composition imply different crystallization environments between wall rocks and pegmatite zones. Based on the geochemistry of apatite samples, it is likely that there is a genetic relationship between the source of muscovite granite and the source of the pegmatite.

Keywords Tetrad effect, Y/Ho ratio, Apatite, Koktokay No. 3 pegmatite

Introduction

Highly fractionated granitic pegmatites are frequently zoned with respect to texture, internal fractionation and mineral assemblages, and these particular granitic rocks are of great interest for their economic potential, being primary sources of Li, Be, Nb, Ta, Cs, ceramic feldspar, gemmologic material and mineralogical specimens. However, the origin and petrogenesis of granitic pegmatites are still highly debated. Currently there are two genetic models to explain the origin of pegmatitic melts: (i) fractionation of igneous intrusions (Jahns and Burnham 1969; Černý 1991; Černý and Ercit 2005; Martin and De Vito 2005; Simmons and Webber 2008) and; (ii) direct anatexis of country rocks (Nabelek et al. 1992a; 1992b; Simmons et al. 1996; Martin and De Vito 2005; Simmons and Webber 2008).

Whole-rock primary chemical compositions, a key constraint on the petrogenesis of pegmatite can be difficult to determine due to complex zoned geometry, coarse mineral grain size and vertical differentiation. Additionally, the elemental and isotopic compositions of whole-rock samples represent only an “average composition” and cannot record the detail of chemical diversity. Therefore, major- and trace-element concentrations, isotopic ratios of minerals and close observation of mineral texture provide pivotal clues to elucidate the evolution and petrogenesis of granitic pegmatite (e.g. Jolliff et al. 1987; Jolliff et al. 1989; Tomascak et al. 1998; Larsen 2002; Larsen et al. 2004; Liu and Zhang 2005; Soares et al. 2008; Zhang et al. 2008a; Zhang et al. 2008b; Sirbescu et al. 2009).

Minerals belonging to the apatite group with the general composition $Ca_5(PO_4)_3(F,Cl,OH)$ (referred to as apatite in this study) are a common accessory phase in igneous, pegmatitic, metamorphic and sedimentary rocks. Apatite is characterized by high contents of REE and other trace elements making it a prime candidate on which to carry out chemical analysis (e.g. Belousova et al. 2002; Liu and Zhang 2005; Chu et al. 2009; Cao et al. 2012). Jolliff et al. (1989) identified a wide variation of REE contents in apatite with the apatite from the pegmatite core containing the lowest REE concentrations. Liu and Zhang (2005) determined the trace element contents of apatite from all nine zones of a pegmatite and confirmed the tetrad effect and non-chondritic Y/Ho ratios in each zone. The tetrad effect and non-chondritic Y/Ho ratios are usually found in highly evolved granite and pegmatite and their associated minerals (e.g. Bau 1996; Irber 1999; Monecke et al. 2002; Liu and Zhang 2005), but not in less evolved granite, mafic rocks and their associated minerals, which indicates different environment and petrogenesis in these two systems. Therefore, the geochemistry of apatite could be used to provide valuable insight into the evolution and petrogenesis of granitic pegmatite.

The Koktokay No.3 pegmatite is a well-known, highly fractionated and zoned granitic pegmatite located in the Altai Mountain, northwestern China. The pegmatite is assumed to be genetically related to the wall rocks constituted by biotite granite and/or two-mica granite/muscovite granite on the basis of spatial proximity (Zou et al. 1986). In this study, major and trace element concentrations in apatite from the pegmatite and from the country rocks have been systematically determined. The objectives of the present work are to investigate the environment of pegmatite and igneous rocks at the time of apatite crystallization and to analyze inter and intra-crystal element variations in apatite during pegmatite crystallization.

Regional geology and sample descriptions

The Koktokay region is situated in the middle of the Altai Orogen and is famous for its abundance of rare metal-bearing pegmatite veins. The Koktokay No.3 pegmatite is located near the town of Koktokay and is the largest Li-Be-Nb-Ta-Cs pegmatite in this area. Three different types of granite, including biotite, two-mica and muscovite varieties, are developed in the mining area and an amphibolite body, which is also referred to as metagabbro pluton, hosts the Koktokay No.3 pegmatite (Fig. 1a). The strata of the Ordovician, Devonian and Carboniferous biotite quartz schist, two-mica schists and staurolite-bearing biotite schist, occur in the west of the mining area (Fig. 1a).

According to the classification of pegmatites (Černý & Ercit, 2005), the Koktokay No.3 pegmatite belongs to the highly fractionated pegmatite LCT family, rare-element class, spodumene subtype. The melt inclusions hosted in beryl, spodumene and quartz from zones I and III homogenize between 700 °C and 900 °C based on microthermometry (Lu et al., 1997), indicating temperature > 700 °C for pegmatite melt zones I and III. In addition, the CO_2-H_2O fluid inclusions hosted in spodumene, quartz and beryl from zones II and VI indicate a pressure of 2.0~3.2 kbar (Wu et al., 1995; Lu et al., 1997), which is equivalent to 6.0~9.6 km, assuming a lithostatic pressure of 3 km/kbar. Zou et al. (1986) systematically studied the O-Pb-Sr isotopes and suggested that the pegmatite magma probably derived from an upper crustal source. Three unpublished Ar-Ar muscovite ages selected from zones of II, IV and VI yielded a consistent age of 180 Ma; this is slightly younger than the 220~198 Ma U-Pb zircon ages published previously (Zhu et al., 2006; Wang et al., 2007b).

The Koktokay No.3 pegmatite is composed of two main parts: a gently dipping “plate” and a steeply dipping “cupola” protruding upwards from the “plate”, resulting in a hat-shaped structure (Fig. 1b, d) (Wang et al. 1981; Zou et al. 1986). The “plate” is fan-like in morphology and extends for 2160 m along a strike of 310° and for 1660 m down dip to the SW at an angle of 10° to 25°. It forms the bottom of the pegmatite at a depth of 200 to 250 m. The “cupola”, the main part of the pegmatite, is a vertical, pipe-like structure, 250×150 m in diameter in the EW section, and plunges steeply at 75° to 90° towards the NE.

Based on the mineral assemblages, textural characteristics and chemical compositions, nine distinct zones with the shape of concentric rings are distinguished in the pegmatitic body (Fig. 1c). From outer to inner, the sequence of these zones is developed as follows (Zou and Li, 2006):

(1) Graphic zone (zone I) (665 m in circumference; 3-7 m in thickness; 220 m in extending depth); mainly composed of microcline and quartz with minor muscovite and surrounded by quartz-muscovite shell.

(2) Saccharoidal albite zone (zone II) (620 m in circumference; 3-6 m in thickness; 220 m in extending depth); consists of 55 vol% microcline, 10 vol% graphic pegmatite, 29 vol% irregular saccaroidal albite, and a muscovite-quartz rim.

(3) Blocky microcline zone (zone III) (580 m in circumference; 0-35 m in thickness; 185 m in extending depth); huge, blocky microcline with an outer contact of saccharoidal albite and inner contact of muscovite-quartz.

(4) Muscovite-quartz zone (zone IV) (520 m in circumference; 4-13 m in thickness; 150 m in extending depth); composed of 60 vol% muscovite-quartz and 30 vol% blocky microcline.

(5) Cleavelandite-spodumene zone (zone V) (400 m in circumference; 3-30 m in thickness; 130 m in extending depth); rich in spodumene, containing 65 vol% cleavelandite-spodumene and 30 vol% quartz-spodumene.

(6) Quartz-spodumene zone (zone VI) (350 m in circumference; 3-5 m in thickness; 100 m in extending depth); contains lithium mineralization, 65 vol% quartz-spodumene and 35 vol% cleavelandite-spodumene.

(7) Platy albite-muscovite zone (zone VII) (280 m in circumference; 5-7 m in thickness; 70 m in extending depth); mainly consisted of platy albite-muscovite with small amount of quartz-spodumene and blocky quartz.

(8) Lepidolite-platy albite zone (zone VIII) (50 m in circumference; 3-7 m in thickness; 15 m in extending depth); lens-shaped, dipping E to NE at an inclination of 75° and mainly composed of lepidolite-platy albite with small amounts of muscovite-platy albite.

(9) Blocky quartz (zone IX) (35-107 m in circumference; 5-40 m in thickness; 80 m in extending depth); comprised of 79 vol% blocky quartz and 21 vol% blocky microcline.

The pegmatite has been systematically described by Wang et al. (1981), Zou et al. (1986) and Zou and Li (2006). In addition, many researchers studied the major composition of the constituent minerals by electron microprobe (Zhang et al., 2004a; 2004b; 2008b; Wang et al., 2006a; 2007a; 2009). However, there is no systematic study of major and trace elements in apatite from the Koktokay No.3 pegmatite. Therefore, twelve apatite samples were selected from each pegmatite zone, except zones III, VII and IX, and also from amphibolite, biotite granite, two-mica granite and muscovite granite, for major and trace elements study. The list of apatite samples and lithology/pegmatite zones are given in Table 1.

Analytical methods

Routine heavy-mineral separation methods have been used to obtain apatite concentrates. Apatite grains with no visible inclusions were handpicked using a binocular microscope, mounted in epoxy blocks and then carefully polished. Polished sections were carbon coated for electron microprobe analysis.

Apatite major-element compositions were measured at the Institute of Geology and Geophysics, Chinese Academy of Sciences (IGGCAS), using a JEOL-JXA8100 electron microprobe (EMP) operated in wavelength dispersive mode (WDS). The operating conditions were 15 kV accelerating voltage, 10 nA beam current and 3μm probe beam with twenty seconds counting time for Si, Al, Fe, Mn, Na and Cl, 40 seconds for F, 10 seconds for P and Ca at their characteristic X-ray line. The following natural minerals and synthetic oxides were used for the calibration: apatite (P), diopside (Ca and Si), jadeite (Al), garnet (Fe), bustamite (Mn), jadeite (Na), tugtupite (Cl), and fluorite (F). All data were corrected using the ZAF procedure described by Henoc and Tong (1978).

The trace-element content of apatite was determined by LA-ICP-MS at the State Key Laboratory of Geological Processes and Mineral Resources, China University of Geosciences (Wuhan) using Geolas 2005. Ion-signal intensities were acquired using an Agilent 7500a ICP-MS instrument with helium (He) as the carrier gas and argon (Ar) as the make-up gas. A 60 μm spot size was employed with each analysis incorporating a 20-30s (gas blank) background acquisition followed by 50s of data acquisition. Detailed analytical technique for the laser ablation system and ICP-MS are described in Hu et al. (2008) and Liu et al. (2008). Calcium content in apatite obtained from EMPA was used as an internal standard to correct matrix effects, signal drift and difference in the ablation yield between sample and reference materials. The external standards used for in-situ analysis of apatite were NIST SRM 610, BCR-2G, BIR-1G and BHVO-2G. Off-line selection, integration of background and analysis signals, time-drift correction and quantitative calibration were performed using ICPMSDataCal (Liu et al. 2008; 2010). The LA-ICP-MS data agree well with the recommended values of the standards (see GeoReM database: http://georem.mpch- mainz.gwdg.de/) and precision is better than 5% for most of the elements. LA-ICP-MS analytical results for international reference materials are listed in the supplementary Spreadsheet 1. Concentrations of major elements determined by EMP and trace elements analyzed by LA-ICP-MS of samples of apatite from Koktokay No. 3 pagmatite are summarized in Table 2. Major and trace elements of whole rocks from Koktokay region are also summarized in the supplementary material.

A brief introduction to the tetrad effect

Before we present the analytical data, it is benificial to briefly review the REE tetrad effect. Fidelis and Siekierski (1966) and Peppard et al. (1969) initially observed the tetrad effect in REE distribution coefficients in certain liquid-liquid extraction systems. The tetrad effect manifests as a split of the chondrite-normalized REE patterns into four segments called tetrads (first tetrad La-Ce-Pr-Nd; second tetrad, (Pm)-Sm-Eu-Gd; third tetrad, Gd-Tb-Dy-Ho; fourth tetrad, Er-Tm-Yb-Lu). Fidelis and Siekierski (1966) and Peppard et al. (1969) suggested that the tetrad effect results from increased stability at quarter, half, three-quarter and complete filling of the 4f electron shell. Several models have been proposed to explain the tetrad effect, including: quantum mechanics where the tetrad effect originates from the interelectron repulsion of electrons in 4f orbitals for trivalent lanthanides (Jørgensen 1970); refined spin-pairing energy theory based on Jørgensen‟s theory (Kawabe 1992) and; the electron configuration model which ultilizes the steric symmetry of configurations of 4f electrons (Masuda et al. 1994). Kawabe et al. (1999) proposed that the direction of the tetrad effect could be explained by the difference in Gibbs free energies of REE species in both phases during the partitioning.

Masuda and Ikeuchi (1979) first observed the lanthanide tetrad effect in natural seawater and phosphorite samples. Moreover, based on theoretical considerations, Masuda et al. (1987) proposed the existence of two „complementary‟ types of tetrad effect: concave W-type in natural waters and related materials, and convex M-type in solid products probably having remained after leaching by an aqueous medium. Masuda and Akagi (1989) initially observed the M tetrad effect in leucogranites collected at Linwu, Hunan Province, China. However, the existence of tetrad effects in geological solid materials is still not widely accepted and is often ascribed to analytical problems or to normalization procedures (McLennan 1994). However, with more and more data obtained using ICP-MS where all REE are determined with high accuracy and sensitivity, tetrad effects are increasingly documented in geosciences, such as in highly evolved igneous rocks (Lee et al. 1994; Bau 1996; Irber 1999; Jahn et al. 2001; Zhao et al. 2002; Wu et al. 2004; Monecke et al. 2007; Yasnygina and Rasskazov 2008; Lee et al. 2010; Peretyazhko and Savina 2010b; Zhao et al. 2010), pegmatite (Bau 1996; Irber 1999; Monecke et al. 2002), chert (Minami et al. 1998), clastic sediments (Liu et al. 1993), meteorites (Inoue et al. 2009), pegmatite minerals (Liu and Zhang 2005), fluorite (Monecke et al. 2002; Wu et al. 2011), zircon (Wu et al. 2011), garnet (Wu et al. 2011) and monazite (Wu et al. 2011), uraninite (Hidaka et al. 1992), kimuraite (Akagi et al. 1993), scheelite (Liu et al. 2007) and xenotime (Masau et al. 2000).

Masuda et al. (1994) and Minami and Masuda (1997) presented a mathematical method to evaluate the degrees of lanthanide tetrad effects. The method of quantification requires that all elements of four tetrads are approximately fitted to a quadratic function and that the resultant quadratic coefficient is employed as a numerical indicator for the degree of the tetrad effect. Irber (1999) proposed an alternative method of quantification to determine the intensity of the tetrad effect. In this case, only the first and the third tetrad are used for quantification of the tetrad effect and only samples with values of $TE_{1,3}>1.10$ are considered. Monecke et al. (2002) put forward a new quantification method that takes into account analytical errors. They consider that significant tetrad effects should have T values exceeding 0.2 for ICP-MS determinations with analytical errors below ±10%.

Results

Major element composition of apatite

Analyzed samples from the wall rocks (amphibolite, biotite granite, two-mica granite and muscovite granite) are obviously different in composition from those in the pegmatite zones (Table 2). Apatite samples from wall rock contains 42.36-43.00 wt% P_2O_5 and 54.03-54.85 wt% CaO, which is higher than those from pegmatite zones which have average values of 42.23-42.72 wt% P_2O_5 and 48.64-53.31 wt% CaO. SiO_2, Al_2O_3, Na_2O and Cl contents are typically below the detection limit. The concentration of FeO shows no variation (with an average of 0.02-0.13 wt%) for all apatites. However, MnO and F contents display a systematic variation (Fig. 2). Wall rock samples show 0.03-0.24 wt% MnO with contents gradually increasing from amphibolite, through biotite granite, two-mica granite and to muscovite granite, whilst almost all apatite samples from pegmatites contain more than 2.00 wt% MnO (except the kh-42 which has an average of 1.04 wt%) (Fig. 2a). All analyzed apatite samples display extremely high F contents ranging from 3.50 to 3.69 wt%, except those from the amphibolite wall rock which show a wider variation (2.48-3.18 wt%; average of 2.70 wt%). Therefore, all apatite crystals can be classified as fluorapatite, except those from amphibolite sample kh-1 (Fig. 2b).

Trace element composition of apatite

Apatite from wall rocks of amphibolite, biotite granite and two-mica granite have high and restricted contents of V and Sr, with average ranging from 5.56 to 8.78 ppm for V and from 140.6 to 262.7 ppm for Sr, while samples from the muscovite granite and pegmatite zones (except of kh-50), show very low contents of V and Sr with contents below detection limit for V and less than 100 ppm for Sr (Fig. 3a). All apatite samples have a wide variation in Y and REE (apatite from wall rocks contain 49.79-2568 ppm Y and REE of 215.4-4106 ppm and apatite from pegmatites contain up to 754 ppm Y and REE of 0.15-3068 ppm) (Fig. 3a). Apatite from wall rocks have higher contents of HREE (Gd to Lu: 41.12-1671 ppm) compared to those from the pegmatite (below detection limit to 271.9 ppm) (Fig 3b), although both groups of apatite have similar LREE contents (La to Eu: mostly 70.00 to 2000 ppm). Apatite from pegmatites display high contents of Th (4.03-652.3 ppm), U (4.03-590.8 ppm) and Pb (8.10-1526.9 ppm), while apatite from wall rocks contain lower contents of Th, U and Pb, with values ranging from 0.35 to 42.36 ppm, 3.39 to 57.57 ppm and 1.13 to 16.59 ppm, respectively (Fig. 3c, d).

The REE patterns of apatite from amphibolite are characterized by upward-convex light rare earth elements (LREE), decreasing chondrite-normalized concentrations from Gd to Lu and negligible Eu anomalies (Fig. 4a). A right inclined REE pattern in apatite may be caused by the crystallization of hornblende (abundant in the rock and in inclusions in apatite) which fractionates the heavy rare earth elements (HREE; Arth and Barker 1976; Green and Pearson 1983) leading to a depleted magma. Apatite crystallizing after hornblende will have low HREE contents.

Apatite from biotite granite kh-69 and two-mica granite kh-66 display similar REE patterns with a relatively flat REE distribution. However, they show different behaviour of Eu with no Eu anomaly in kh-69 and negative Eu anomaly in kh-66 (Fig. 4b, c). The lack of an apatite Eu anomaly in kh-69 apatite reflects apatite crystallization prior to plagioclase, while obvious negative Eu anomalies in kh-66 apatite are probably caused by early crystallization of plagioclase before apatite. Because, Eu shows similar geochemical behaviour to Sr (Drake and Weill 1975), crystallization of plagioclase will deplete Sr and Eu from the magma, and cause low contents of Sr and Eu in late apatite. This is consistent with lower contents of Sr in apatite from kh-66 than samples from kh-69 (Fig. 3a).

All other apatites, including that from muscovite granite and different zones of pegmatite, show kinked REE patterns, which are called tetrad effects (Fig. 4) and obvious negative Eu anomalies

(Eu/Eu* values mainly changing from 0.02 to 0.10) except apatite from kh-30 which displays both positive and negative Eu anomalies. Apatite from the muscovite granite show $(La/Yb)_N < 0.60$ with ratios ranging from 0.16 to 0.57, whilst all pegmatite apatites have $(La/Yb)_N > 2$ with the majority ranging from 10 to 50.

Tetrad effect

In this study, we calculated the size of the lanthanide tetrad effect in apatite using the methods described by Irber (1999) and Monecke et al. (2002). The frequency distributions of the obtained T and $TE_{1,3}$ values are given in Fig. 5. The calculated T and $TE_{1,3}$ for the REE patterns of the apatite from the biotite granite kh-69 and two-mica granite kh-66 are lower than 0.2 and 1.1, respectively (Fig. 5a, c), which indicates that the apatite from these two samples (and the host rock) do not show significant tetrad effects. In contrast, apatite from the amphibolite has a wide range of T and $TE_{1,3}$ (0.11 to 0.35 and 1.00 to 1.21, respectively) (Fig. 5a, c), which may be caused by the upward-convex LREE patterns or by alteration. Although Liu and Zhang (2005) showed that strongly altered amphibolites collected at the quenched boundary with the pegmatite displays a well defined tetrad effect, our sample is relatively fresh with no tetrad effect found in its host rock, which may suggest that the upward-convex LREE pattern causes the wide distribution of T and $TE_{1,3}$ for the apatite in this study. All apatite samples collected in the muscovite granite kh-70 and pegmatite units show a well developed tetrad effect with values of T ranging from 0.2 to 0.4 for muscovite granite and from 0.3 to 0.8 for pegmatite zones and $TE_{1,3}$ from 1.2 to 1.4 and from 1.2 to 1.8 for muscovite granite and pegmatite zones, respectively (Fig. 5). Moreover, the whole rock analyses from muscovite granite and pegmatite zone I to zone IV display obvious tetrad effects (Fig. 4), while the whole rock analyses from pegmatite zone V to IX do not show tetrad effects due to very low contents of REE (Fig. 4).

Discussion

REE tetrad effect

Several genetic models have been proposed to explain the origin of the tetrad effect in geological samples: (1) surface weathering (Masuda and Akagi 1989; Takahashi et al. 2002); (2) fractional crystallization of individual mineral phases (Yurimoto et al. 1990; Zhao and Cooper 1993; McLennan 1994; Pan 1997; Pan and Breaks 1997); (3) fluid-melt interaction (Kawabe 1995; Irber 1999; Dolejš and Štemprok 2001; Zhao et al. 2002; Monecke et al. 2007) and; (4) immiscible fluoride and silicate melts (Veksler et al. 2005; Badanina et al. 2006; Peretyazhko and Savina 2010a). Each will be considered in the context of the data obtained here.

Surface weathering

Masuda and Akagi (1989) and Takahashi et al. (2002) suggested that if groundwater with a concave tetrad effect interacts with granitic rocks during weathering processes, those granites will inherit the tetrad effect from the protolith. However, our pegmatite samples are quite fresh and it is therefore unlikely that surface weathering contributed to the tetrad effect observed in the studied apatite samples.

Fractional crystallization of individual mineral phases

The fractional crystallization model implies that the kinked shape of chondrite-normalized REE patterns is caused by conventional magmatic crystallization of minerals. For example, the discontinuity between Nd and Pm is attributed to fractional crystallization of monazite (Yurimoto et al. 1990; Zhao and Cooper 1993; Pan and Breaks 1997), the discontinuity between Ho and Er is attributed to fractional crystallization of Y-rich accessory minerals, such as garnet (Pan 1997; Pan and

Breaks 1997) and the discontinuity between Gd and Tb is interpreted to be produced by apatite fractional crystallization (McLennan 1994). However, according to Bau (1997) and Irber (1999), even for random mineral combinations, the known partition coefficients do not result in tetrad effects in the REE pattern. Furthermore, accessory minerals including garnet, monazite, xenotime and apatite typically show similar tetrad effects in their REE patterns as the granitic host rocks (Masau et al. 2000; Liu and Zhang 2005; Wu et al. 2011); this rules out the whole rock samples acquiring their convex tetrads during fractional crystallization. As seen on Fig. 4 both the apatite and whole rock exhibit similar REE patterns, both with significant tetrad effect. Hence, fractionation of minerals to produce the tetrad effect can be ruled out.

Fluid-melt interaction

Kawabe (1995), Irber (1999), Dolejš and Štemprok (2001) and Zhao et al. (2002) suggested that fluid-melt interactions can induce a convex tetrad effect in whole-rock during late crystallization stages of silicate melts in an open system, which requires immiscible fluid with complementary concave tetrad effect moving out from the residual solidified magma. Jahn et al. (2001) and Wu et al. (2004) suggested that the intense interaction of residual melts with aqueous hydrothermal fluids enhance the tetrad effect in REE distribution patterns and non-CHARAC trace element behavior during late stage magmatic evolution. The former studies showed that groundwater, seawater and their precipitates (such as phosphorite, chert, shell, uraninite and sedimentary rocks) often display W-type lanthanide tetrad effect (Masuda and Ikeuchi 1979; Hidaka et al. 1992; Minami et al. 1998; Takahashi et al. 2002). However, Monecke et al. (2002) and Badanina et al. (2006) reported that vein fluorite precipitated from hydrothermal fluid shows a well developed convex tetrad effect. Moreover, Liu and Zhang (2005) indicated that the strongly altered amphibolite, as the direct wall rock of the Koktokay No. 3 pegmatite, displays a convex tetrad effect, and Monecke et al. (2007) discovered that rhyolite samples replaced by albitizing fluids which are exsolved from the magma, show a well developed convex tetrad effect. These observations suggest that hydrothermal fluids derived from granitic magma do not display W-type tetrad effect, but, on the contrary, show M-type tetrad effect.

Fluids with characteristic convex tetrad effect exsolved from magma are, therefore, unlikely to erase the concave tetrad effect REE patterns and leave the residual solidified magma with a convex tetrad effect.

Immiscible fluoride and silicate melts

Silicate magmas become saturated in volatiles and exsolve a broad spectrum of volatile phases including aqueous, aqueous-carbonic, and aqueous-sulfate vapors or liquids as well as sulfide, carbonate, phosphate, and/or hydrosaline (Cl- and/or F-rich) liquids or melts (e.g. see Webster 2004). Hydrosaline fluorine melts, which under certain conditions, are equivalent to fluoride melt (Webster 2004; Veksler et al. 2005; Badanina et al. 2006; Peretyazhko and Savina 2010b), are high temperature melts, which are, F-rich (up to 50 wt%, or even higher) but H_2O- and Si-poor.

Veksler et al. (2005) first conducted high-temperature experiments in F-rich systems and found immiscible fluoride melts containing very high concentrations of lanthanides and Y and non-chondritic Y/Ho. In addition, there was a concave tetrad effect for REE partition coefficients between fluorides melt and silicate melts. They proposed that non-chondritic Y/Ho and lanthanide tetrad effects of whole rock are likely to be caused by interaction of immiscible fluoride melts and silicate melts. Badanina et al. (2006) and Peretyazhko and Savina (2010b) also attributed the well developed convex tetrad effects of residual magma to the separation of the immiscible fluoride melts with W-type tetrad effects from silicate melts.

Products of fluoride melts have been reported in ongonite (a kind of Li- and F-bearing rare metal granite) (Peretyazhko et al. 2007; Peretyazhko and Savina 2010a) and in metasomatized xenoliths (Klemme 2004). Recently, Dolejš and Baker (2004; 2007a; 2007b) systematically investigated phase equilibria in the systems of Na_2O-K_2O-CaO-Al_2O_3-SiO_2-H_2O-F_2O_{-1}, K_2O-Na_2O-Al_2O_3-SiO_2-F_2O_{-1}-H_2O and K_2O-Na_2O-Al_2O_3-SiO_2-F_2O_{-1}-H_2O to define the location of fluoride-silicate liquid immiscibility and outlined differentiation paths of fluorine-bearing silicic magmas. They proposed that the sequential formation of fluorides can be expressed by the chemical potential $\mu(F_2O_{-1})$ which is buffered by the reaction: $MO_{n/2}$ (s)+n/2[F_2O_{-1}]=MF_n (s, g) where M=K, Na, Ca, Al, Si. For example, topaz and cryolite are stable solid phases in calcium-poor systems, however, the presence of calcium may cause the crystallization of fluorite.

The Koktokay No.3 pegmatite is a highly evolved granite pegmatite, rich in Li, B, F, P, Cl and H_2O. Accessory to minor topaz was reported in each pegmatite zone, except from core zone IX (blocky quartz and microcline core); it is more commonly distributed in zones IV (muscovite-quartz zone) and VIII (lepidolite-platy albite zone; Zou and Li 2006). This indicates a high F concentration in the pegmatitic melt. In addition, all apatite samples from pegmatite are characterized by high contents of F (Fig. 6b), and F-rich lepidolite (up to 7.30 wt% F) was also reported by Wang et al. (2007a).

Piccoli and Candela (1994) and Piccoli et al. (1999) developed a model to estimate the concentrations of HF and F in magmatic vapor and melt from apatite and host rock chemistry:

$$C_F^{vap} = \frac{X(Fap)}{X(Hap)} \times \frac{1.90\times10^7}{18} \times \frac{1}{10^{[0.18219+\frac{5301.1-0.0036\times(P-1)}{T+273}]}} ;$$

and $C_F^{mel} = \dfrac{C_F^{vap}}{D^{vap/mel}}$;

Where $D_F^{vap/mel} = -0.56 + 0.00093\times T$ is vapor/melt distribution coefficient for F from Webster (1990), $T = \dfrac{264\times C_{SiO_2} - 4800}{[0.124\times C_{SiO_2} - \ln(C_{P_2O_5}/100) - 3.97]} - 273$ is the temperature of saturation of apatite (in °C) from Harrison and Watson (1984), P is pressure of apatite crystallization (in bar), X(Fap), X(Hap) are mole fractions of fluorapatite, hydroxylapatite and C_{SiO2}, C_{P2O5} are SiO_2 and P_2O_5 wt% from the whole rock analysis. Assuming a pressure of 3000 bar, 1.65, 1.43 and 2.83 wt% of F in the melts of biotite granite, two-mica granite and muscovite granite, respectively are obtained. Contents of F in the melts of amphibolite and pegmatite zones have not been calculated because amphibolite is relatively altered and the representative bulk chemical compositions of pegmatite are difficult to determine. In fact, the effect of pressure on F contents in the melts is negligible. For example, with pressure changing from 2000 to 4000 bar, the concentrations of F in melts of biotite granite, two-mica granite and muscovite granite vary only from 1.63 to 1.67 wt%, 1.41 to 1.45 wt% and 2.80 to 2.87 wt%, respectively. 2.83 wt% of F in muscovite granite is higher than that of biotite granite and two-mica granite, and the concentrations of F in the pegmatite zones should be > 2.83 wt% because of their highly evolved features.

Therefore, these high F granitic melts likely gave rise to immiscible fluoride, which contributes to the complementary M-type tetrad effect of the residual melt and minerals forming from them such as apatite, spessartite, tourmaline, beryl and alkali feldspar.

Non-CHARAC Y/Ho and Eu depletion

For typical silicate melt systems, CHARAC (CHArge-and-Radius-Controlled) behavior of Zr and Hf, Y and Ho is observed on melts of basic to intermediate composition, and basic to intermediate igneous rocks show Y/Ho and Zr/Hf ratios which are close to the chondritic ratios with ratios of Y/Ho 24-34 and Zr/Hf 26-46 (Bau 1996). In contrast, the behavior of Zr and Hf, Y and Ho in highly evolved magmas is distinctly different to those of basic to intermediate composition; rather, it resembles trace element behavior in aqueous media because these elements may form complexes with a variety of ligands such as non-bridging oxygen (NBO), F, B, etc. (Ponader and Brown Jr 1989; Keppler 1993; Bau 1996). Therefore, non-CHARAC behavior is a reflection of specific physicochemical properties of the magma. It is characteristic for high-silica magmatic systems (e.g., pegmatite) rich in H_2O, Li, B, F, P and/or Cl with a transitional behavior between pure silicate melts and hydrothermal fluids (Bau 1996).

Non-CHARAC Y/Ho ratios are found in apatite samples from pegmatite with values of Y/Ho ranging from 40 to 120, while, apatite from the muscovite granite show chondritic Y/Ho ratios (Y/Ho: 25.8 to 28.3) (Fig. 6a) In contrast, apatite from muscovite granite and pegmatite zones all display well developed tetrad effects (Fig. 6a). This decoupling may suggest that the origins of tetrad effects and non-CHARCA Y/Ho are different, and that the crystallization of pegmatite zones are probably accompanied by large amounts of hydrothermal fluid exsolved from the silicate melt, whereas lesser amounts of fluid were exsolved from the muscovite granite melt during granite crystallization. This is consistent with the opinion of Peretyazhko and Savina (2010b), who suggested that the influence of high-temperature F- and Cl-bearing fluids on silicate melts produces an increase in Y/Ho ratio owing to the elevated solubility of Ho in such fluids.

Most apatite samples from the pegmatite show extreme negative Eu anomalies with values of Eu/Eu* changing from 0.02 to 0.10. Although negative Eu anomalies are commonly explained by feldspar fractionation, Irber (1999) showed that extremely low Eu/Eu* (<0.06) could not be produced by Reyleigh fractionation. Abramov (2001) suggested that the high solubility of Eu compared with other REEs in F- and Cl-bearing aqueous fluids ($\sim 10^{-2}$ mol/kg) at 500-800 °C, could be responsible for the extreme negative Eu anomaly in granite rocks and minerals. This possible explanation was proposed by Muecke and Clarke (1981) who suggested that strong Eu depletion in late-stage granite may indicate a preferential Eu partitioning into co-existing hydrothermal fluids rather than into feldspar. Moreover, on the basis of theoretical calculation, Candela (1990) confirmed that strong separation of divalent Eu from the trivelant REE can easily be explained by REE preferential partitioning between a silicate melt and an exsolved hydrothermal fluid.

Therefore, non-CHARAC Y/Ho ratios and extreme negative Eu anomalies in apatite samples from the Koktokay No. 3 pegmatite are likely caused by the abundance of fluid exsolved from the pegmatite melts.

Inter and intra-crystal element variations in apatite

Three levels of different element distribution have been identified: (1) within a single crystal; (2) between different crystals in the same sample and/or pegmatite zones and; (3) between crystals from different samples and/or pegmatite zones.

Variations within a single crystal

Distribution of the major and trace elements, including CaO, P_2O_5, MnO, F, Sr, Y, La, Ce, Yb, in a traverse of a single apatite crystal from different samples, is shown in Figure 7.

All major elements, except CaO and MnO, show relatively homogeneous distribution within a single apatite crystal (Fig. 7). The concentrations of MnO and CaO in apatite samples kh-42-21, kh-44-1, kh-52-23, kh-54-3, kh-50-8 and kh-65-4 show complementary relationships (Fig. 7), which implies that Mn substitutes for Ca in the apatite lattice. The substitution of Mn for Ca is evidenced by the perfect positive correlation between Mn and Ca (Hughes et al. 1991; Fig. 8). Apatite from zones IV to VIII show a high variation of MnO concentrations, which is likely linked to the crystallization of Mn-bearing minerals belonging to the columbite group; the latter are common accessory minerals in zones II to VIII (Zhang et al. 2004b) and tiny inclusions of columbite group minerals were detected by backscattered electron (BSE) imaging in apatite.

Most apatite grains show relatively uniform concentrations of trace elements, suggesting relatively homogeneous melt composition during single apatite grain crystallization, while large variations of trace elements within a single apatite crystal are observed in kh-69-17, kh-66-13, kh-44-1 and kh-52-23 (Fig. 7). Variations of local melt composition during apatite crystallization may be the main reason for the variations seen in grains kh-69-17 and kh-66-13. For example, kh-66-13 shows clear oscillatory zoning on BSE images (Fig. 7). Tepper and Kuehner (1999) suggested that the zoning of apatite is attributed to changes in melt composition resulting from magma mixing and differentiation. Concentrations of REE in the bright zone of BSE are higher than in the dark zones, which is in accordance with kh-66-13 (spot 5 in the bright zone with REE value of 3344 ppm and spot 8 in the dark zone with REE value of 2160 ppm). For kh-44-1, anomalously high La and Ce in spots 9 and 11 are likely caused by tiny monazite inclusions which show a preference for LREEs (Yurimoto et al. 1990). This is consistent with higher LREEs in spots 9 and 11 (406 ppm and 383 ppm) than other spots (from 338 to 346 ppm); the HREE concentrations are similar for all spots (6.13 to 6.69 ppm). In addition, tiny monazite grains are found as mineral inclusions in other apatite grains in kh-44. The lowest concentrations of REE+Y in the core of grain kh-52-23 are possibly caused by the crystallization of uranmicrolite associated with apatite. Uranmicrolite, as an abundant accessory mineral in pegmatite zones V to VIII (Zou and Li 2006) and it can accommodate significant concentrations of lanthanides (Lumpkin et al. 1986). It was also detected as inclusion in apatite in sample kh-52.

Variations between different crystals in the same sample and/or pegmatite zones

The F values of apatite from the amphibolite range from 2.48 to 3.18 wt%. This wide variation may imply that the whole rock was affected by the alteration of hydrothermal fluids released from the pegmatite melt. This is supported by the observation that amphibolite adjacent to the contact is characterized by an alteration halo of Li, Rb, Cs, F and B. With a few exceptions, the F values of apatite from other samples vary by less than 0.45 wt%; i.e. 3.30 to 3.75 wt% for most apatite from granite and pegmatite. Restricted variations of Mn, Pb, Th and Y are found in wall rocks (Figs. 2a, 9a-c). However, substantial variability of Mn, Pb, Th and Y occurs among apatite from pegmatite zones (Figs. 2a, 9a-c): 0.14 to 7.88 wt% for MnO; 8.10 to 456 ppm for Pb; 4.03 to 652 ppm for Th and; below limit of detection to 755 ppm for Y. The large differences in the element distribution of apatite between wall rocks and pegmatite zones suggest that different crystallization environments existed.

Variations between crystals from different samples and/or pegmatite zones

There appears to be a progressive increase in Pb content in apatite from amphibolite to biotite granite, two-mica granite and muscovite granite and from the outer pegmatite to the inner zones (Fig. 9a). However, variations of other elements and element ratios, such as Th, Y, REE, Sr/Y and Y/Ho, show totally different patterns in wall rock and in pegmatite zones (Fig. 9). Contents of Sr, Th and U and Sr/Y ratios in apatite samples display a progressive decrease from wall rock (in the sequence of amphibolite → biotite granite → two mica granite → muscovite granite), but a progressive increase and/or no change from the pegmatite rim to the core (Fig. 9b, e). Y and REE contents in apatite show gradual increase in wall rocks then progressive decrease from the pegmatite rim to the core (Fig. 9c, d). These different evolution trends suggest distinct physico-chemical conditions during apatite crystallization. Fig. 9f shows non-CHARAC Y/Ho and a progressive increase of Y/Ho from the pegmatite margin to the core, in contrast to the nearly chondritic Y/Ho values of the wall rocks, ranging from 24 to 34. Non-CHARAC behavior of Y/Ho has been discussed above and is a reflection of specific physicochemical properties of the transitional magma between pure silicate melts and hydrothermal fluids (Bau 1996). Greater deviations of Y/Ho from the chondrite value of 28.1 (Anders and Grevesse 1989) in apatite from the inner zones of the pegmatite may reflect the specific physico-chemical property of the hydrothermal fluid. The steady increase of Pb from wall rock to pegmatite zones may suggest that the behavior of Pb is similar in (transitional) silicate melts and in hydrothermal fluids. However, other elements such as Th, U, Y and REE display very different behavior in melts vs. fluids. Decreasing concentrations of Sr, Th and Sr/Y in apatite and increasing concentrations of Y and REE in apatite are directly correlated with the concentrations of these elements in the melts, which may in turn be related to the degree of magmatic fractionation. This is consistent with the results of Belousova et al. (2001; 2002), Chu et al. (2009) and Cao et al. (2012) who demonstrated that Sr concentrations decrease with magma fractionation, while Y concentrations increase. The low concentrations of REE and Y in apatite samples from the inner zones of the pegmatite are likely caused by the crystallization of uranmicrolite, further supported by large amounts of uranmicrolite occurring in the inner zones (Lumpkin et al. 1986; Zou and Li 2006).

Conclusions

(1) The tetrad effect observed in apatite from the muscovite granite and the pegmatite zones of Koktokay No. 3 pegmatite are most likely produced by the interaction of immiscible fluoride and silicate melts, rather than by weathering, fractional crystallization of individual mineral phases and/or fluid-melt interaction.

(2) Non-CHARAC Y/Ho ratios and extremely negative Eu anomalies in apatite are likely caused by magmatic-hydrothermal fluids exsolved from the pegmatite melts.

(3) Apatite samples from muscovite granite display well developed tetrad effects together with chondritic Y/Ho ratios. This suggests different origins for tetrad effects and non-CHARCA Y/Ho ratios.

(4) Variations of major and trace elements in apatite are attributed to several factors including the evolution of melt composition and the crystallization of other accessory minerals.

(5) Apatite compositions indicate different crystallization conditions of apatite in the wall rocks and in the pegmatite zones. They are more similar between muscovite granite and pegmatite.

Acknowledgments

The authors are greatly indebted to Dr. Qian Mao and Mr. Yu-Guang Ma for their assistance with EPM analyses and Yong-Sheng Liu for assistance with LA-ICP-MS analyses at the State Key Laboratory of Geological Processes and Mineral Resources, China University of Geosciences (Wuhan). The manuscript was improved by the thoughtful comments of Wang Xuan-Ce, Lynette Howearth and Laurie Burn Nunes. In particular, we express our gratitude to two anonymous reviewers for their constructive comments and excellent suggestions that helped to improve the manuscript. This research was financially supported by Knowledge Innovation Project of Chinese Academy of Sciences (Grant number KZCX2-YW-Q04-08) and Ministry of Land and Resources Comprehensive Research for Typical Mineral Deposits (Grant number 20089932).

References

Abramov SS (2001) Modeling of REE fractionation in the acid melt-fluoride-chloride fluid system. Dokl Earth Sci 377:198−200

Akagi T, Shabani MB, Masuda A (1993) Lanthanide tetrad effect in kimuraite [$CaY_2(CO_3)_4·6H_2O$]: Implication for a new geochemical index. Geochim Cosmochim Acta 57:2899−2905

Anders E, Grevesse N (1989) Abundances of the elements: Meteoritic and solar. Geochim Cosmochim Acta 53:197−214

Arth JG, Barker F (1976) Rare-earth partitioning between hornblende and dacitic liquid and implications for the genesis of trondhjemitic-tonalitic magmas. Geology 4:534−536

Badanina EV, Trumbull R B, Dulski P, Wiedenbeck M, Veksler IV, Syritso LF (2006) The behavior of rare-earth and lithophile trace elements in rare-metal granites: a study of fluorite, melt inclusions and host rocks from the Khangilay complex, Transbaikalia, Russia. Can Mineral 44:667−692

Bau M (1996) Controls on the fractionation of isovalent trace elements in magmatic and aqueous systems: evidence from Y/Ho, Zr/Hf and lanthanide tetrad effect. Contrib Mineral Petrol 123:323−333

Bau M (1997) The Lanthanide tetrad effect in highly evolved felsic igneous rocks: a reply to the comment by Y. Pan. Contrib Mineral Petrol 128:409−412

Belousova EA, Griffin WL, O'Reilly SY, Fisher NI (2002) Apatite as an indicator mineral for mineral exploration: trace-element compositions and their relationship to host rock type. J Geochem Explor 76:45−69

Belousova EA, Walters S, Griffin WL, O'Reilly SY (2001) Trace-element signatures of apatites in granitoids from the Mt Isa Inlier, northwestern Queensland. Aust J Earth Sci 48:603−619

Bizzarro M, Simonetti A, Stevenson RK, Kurszlaukis S (2003) In situ $^{87}Sr/^{86}Sr$ investigation of igneous apatites and carbonates using laser-ablation MC-ICP-MS. Geochim Cosmochim Acta 67:289−302

Candela PA (1990) Theoretical constraints on the chemistry of the magmatic aqueous phase. In: Stein HJ, Hannah JL (eds) Ore-bearing granite systems, petrogenesis and mineralizaing processes. Geol Soc Am, Special Paper 246:11−19

Cao MJ, Li GM, Qin KZ, Seitmuratova EY, Liu YS (2012) Major and trace element characteristics of apatites in granitoids from Central Kazakhstan: Implications for petrogenesis and mineralization. Resour Geol 62:63−83

Černý P (1991) Rare-element granitic pegmatites. Part II: Regional to global environments and petrogenesis. Geosci Can 18:68−81

Černý P, Ercit TS (2005) The classification of granitic pegmatites revisited. Can Mineral 43:2005−2026

Chen FW, Li HQ, Wang DH, Cai H, Chen W (2000) New data on the Yanshanian chronology of ore-forming in Altay Mountains. Chin Sci Bull 44:1142−1148

Chu M. Wang K, Griffin W, Chung S, O'Reilly S, Pearson N, Iizuka Y (2009) Apatite composition: tracing petrogenetic processes in Transhimalayan granitoids. J Petrol 50:1829−1855

Dolejš D, Baker DR (2004) Thermodynamic analysis of the system Na_2O-K_2O-CaO-Al_2O_3-SiO_2-H_2O- F_2O_{-1}: Stability of fluorine-bearing minerals in felsic igneous suites. Contrib Mineral Petrol 146:762−778

Dolejš D, Baker DR (2007a) Liquidus Equilibria in the System K_2O-Na_2O-Al_2O_3-SiO_2-F_2O_{-1}-H_2O to

100 MPa: II. Differentiation paths of fluorosilicic magmas in hydrous systems. J Petrol 48:807−828

Dolejš D, Baker DR (2007b) Liquidus equilibria in the system K_2O-Na_2O-Al_2O_3-SiO_2-F_2O_{-1}-H_2O to 100 MPa: I. Silicate-fluoride liquid immiscibility in anhydrous systems. J Petrol 48:785−806

Dolejš D, Štemprok M (2001) Magmatic and hydrothermal evolution of Li-F granites: Cínovec and Krásno intrusions, Krušné hory batholith, Czech Republic. Bull Geosci 76:77−99

Drake MJ, Weill DF (1975) Partition of Sr, Ba, Ca, Y, Eu^{2+}, Eu^{3+} and other REE between plagioclase feldspar and magmatic liquid: an experimental study. Geochim Cosmochim Acta 39:689−712

Fidelis I, Siekierski S (1966) The regularities in stability constants of some rare earth complexes. J Inorg Nucl Chem 28:185−188

Foster GL, Carter A (2007) Insights into the patterns and locations of erosion in the Himalaya - A combined fission-track and *in situ* Sm-Nd isotopic study of detrital apatite. Earth Planet Sci Lett 257:407−418

Foster GL, Vance D (2006) *In situ* Nd isotopic analysis of geological materials by laser ablation MC-ICP-MS. J Anal At Spectrom 21:288−296

Green T, Pearson N (1983) Effect of pressure on rare earth element partition coefficients in common magmas. Nature 305:414−416

Gregory CJ, McFarlane CRM, Hermann J, Rubatto D (2009) Tracing the evolution of calc-alkaline magmas: In-situ Sm-Nd isotope studies of accessory minerals in the Bergell Igneous Complex, Italy. Chem Geol 260:73−86

Harrison TM, Watson EB (1984) The behavior of apatite during crustal anatexis: Equilibrium and kinetic considerations. Geochim Cosmochim Acta 48:1467−1477

Henderson AL, Foster GL, Najman Y (2010) Testing the application of in situ Sm-Nd isotopic analysis on detrital apatites: A provenance tool for constraining the timing of India-Eurasia collision. Earth Planet Sci Lett 297:42−49

Henoc J, Tong M (1978) Automatisation de la microsonde. J Microsc Spectrosc Electr 3:247−254

Hidaka H, Holliger P, Shimizu H, Masuda A (1992) Lanthanide tetrad effect observed in the Oklo and ordinary uraninites and its implication for their forming processes. Geochem J 26:337−346

Hu ZC, Gao S, Liu YS, Hu SH, Chen HH, Yuan HB (2008) Signal enhancement in laser ablation ICP-MS by addition of nitrogen in the central channel gas. J Anal At Spectrom 23:1093−1101

Hughes JM, Cameron M, Crowley KD (1991) Ordering of divalent cations in the apatite structure; crystal structure refinements of natural Mn-and Sr-bearing apatite. Am Miner 76:1857−1862

Inoue M, Nakamura N, Kimura M (2009) Tetrad effects in REE abundance patterns of chondrules from CM meteorites: Implications for aqueous alteration on the CM parent asteroid. Geochim Cosmochim Acta 73:5224−5239

Irber W (1999) The lanthanide tetrad effect and its correlation with K/Rb, Eu/Eu*, Sr/Eu, Y/Ho and Zr/Hf of evolving peraluminous granite suites. Geochim Cosmochim Acta 63:489−508

Jørgensen CK (1970) The "Tetrad effect" of Peppard is a variation of the nephelauxetic ratio in the third decimal. J Inorg Nucl Chem 32:3127−3128

Jahn BM, Wu FY, Capdevila R, Martineau F, Zhao ZH, Wang YX (2001) Highly evolved juvenile granites with tetrad REE patterns: the Woduhe and Baerzhe granites from the Great Xing'an Mountains in NE China. Lithos 59:171−198

Jahns RH, Burnham CW (1969) Experimental studies of pegmatite genesis; l, A model for the derivation and crystallization of granitic pegmatites. Econ Geol 64:843−864

Jolliff BL, Papike JJ, Laul JC (1987) Mineral recorders of pegmatite internal evolution: REE contents of tourmaline from the Bob Ingersoll pegmatite, South Dakota. Geochim Cosmochim Acta 51:2225−2232

Jolliff BL, Papike JJ, Shearer CK, Shimizu N (1989) Inter- and intra-crystal REE variations in apatite from the Bob Ingersoll pegmatite, Black Hills, South Dakota. Geochim Cosmochim Acta 53:429−441

Kawabe I (1992) Lanthanide tetrad effect in the Ln^{3+} ionic radii and refined spin-pairing energy theory. Geochem J 26:309−335

Kawabe I (1995) Tetrad effects and fine structures of REE abundance patterns of granitic and rhyolitic rocks: ICP-AES determinations of REE and Y in eight GSJ reference rocks. Geochem J 29:213−230

Kawabe I, Ohta A, Ishii S, Tokumura M, Miyauchi K (1999) REE partitioning between Fe-Mn oxyhydroxide precipitates and weakly acid NaCl solutions: Convex tetrad effect and fractionation of Y and Sc from heavy lanthanides. Geochem J 33:167−180

Keppler H (1993) Influence of fluorine on the enrichment of high field strength trace elements in granitic rocks. Contrib Mineral Petrol 114:479−488

Klemme S (2004) Evidence for fluoride melts in Earth's mantle formed by liquid immiscibility. Geology 32:441−444

Larsen RB (2002) The distribution of rare-earth elements in K-feldspar as an indicator of petrogenetic processes in granitic pegmatites: examples from two pegmatite fields in southern Norway. Can Mineral 40:137−152

Larsen RB, Henderson I, Ihlen PM, Jacamon F (2004) Distribution and petrogenetic behaviour of trace elements in granitic pegmatite quartz from South Norway. Contrib Mineral Petrol 147:615−628

Lee SG, Asahara Y, Tanaka T, Kim NH, Kim KH, Yi K, Masuda A, Song YS (2010) La-Ce and Sm-Nd isotopic systematics of early Proterozoic leucogranite with tetrad REE pattern. Chem Geol 276:360−373

Lee SG, Masuda A, Kim HS (1994) An early Proterozoic leuco-granitic gneiss with the REE tetrad phenomenon. Chem Geol 114:59−67

Little JEJ, Jones MM (1960) A complete table of electronegativities. J Chem Educ 37:231−233

Liu CQ, Masuda A, Okada A, Yabuki S, Zhang J, Fan ZL (1993) A geochemical study of loess and desert sand in northern China: Implications for continental crust weathering and composition. Chem Geol 106:359−374

Liu CQ, Zhang H (2005) The lanthanide tetrad effect in apatite from the Altay No. 3 pegmatite, Xingjiang, China: an intrinsic feature of the pegmatite magma. Chem Geol 214:61−77

Liu Y, Deng J, Li CF, Shi GH, Zheng AL (2007) REE composition in scheelite and scheelite Sm-Nd dating for the Xuebaoding W-Sn-Be deposit in Sichuan. Chin Sci Bull 52:2543−2550

Liu Y, Gao S, Hu Z, Gao C, Zong K, Wang D (2010) Continental and oceanic crust recycling-induced melt-peridotite interactions in the Trans-North China Orogen: U-Pb Dating, Hf isotopes and trace elements in zircons from mantle xenoliths. J Petrol 51:537−571

Liu Y, Hu Z, Gao S, Gunther D, Xu J, Gao C, Chen H (2008) In situ analysis of major and trace elements of anhydrous minerals by LA-ICP-MS without applying an internal standard. Chem Geol 257:34−43

Lu HZ, Wang ZG, Li YS (1997) Magma-fluid transition and the genesis of pegmatite dike No. 3, Altay, Xinjiang, Northwest China. Chin J Geochem 16:43–52

Lumpkin GR, Chakoumakos BC, Ewing RC (1986) Mineralogy and radiation effects of microlite from the Harding Pegmatite, Taos County, New Mexico. Am Miner 71:569–588

Martin RF, De Vito C (2005) The patterns of enrichment in felsic pegmatites ultimately depend on tectonic setting. Can Mineral 43:2027–2048

Masau M, Černý P, Chapman R (2000) Dysprosian Xenotime-(Y) from the Annie Claim #3 granitic pegmatite, Southeastern Manitoba, Canada: evidence of the tetrad effect? Can Mineral 38:899–905

Masuda A, Akagi T (1989) Lanthanide tetrad effect observed in leucogranites from China. Geochem J 23:245–253

Masuda A, Ikeuchi Y (1979) Lanthanide tetrad effect observed in marine environment. Geochem J 13:19–22

Masuda A, Kawakami O, Dohmoto Y, Takenaka T (1987) Lanthanide tetrad effects in nature: two mutually opposite types, W and M. Geochem J 21:119–124

Masuda A, Matsuda N, Minami M, Yamamoto H (1994) Approximate estimation of the degree of lanthanide tetrad effect from precise but partially void data measured by isotope dilution and an electron configuration model to explain the tetrad phenomenon. Proc Japan Acad 70B:169–174

McFarlane CRM, McCulloch MT (2007) Coupling of in-situ Sm-Nd systematics and U-Pb dating of monazite and allanite with applications to crustal evolution studies. Chem Geol 245:45–60

McLennan SM (1994) Rare earth element geochemistry and the "tetrad" effect. Geochim Cosmochim Acta 58:2025–2033

Minami M, Masuda A (1997) Approximate estimation of the degree of lanthanide tetrad effect from the data potentially involving all lanthanides. Geochem J 31:125–134

Minami M, Masuda A, Takahashi K, Adachi M, Shimizu H (1998) Y-Ho fractionation and lanthanide tetrad effect observed in cherts. Geochem J 32:405–420

Monecke T, Dulski P, Kempe U (2007) Origin of convex tetrads in rare earth element patterns of hydrothermally altered siliceous igneous rocks from the Zinnwald Sn-W deposit, Germany. Geochim Cosmochim Acta 71:335–353

Monecke T, Kempe U, Monecke J, Sala M, Wolf D (2002) Tetrad effect in rare earth element distribution patterns: a method of quantification with application to rock and mineral samples from granite-related rare metal deposits. Geochim Cosmochim Acta 66:1185–1196

Muecke GK, Clarke DB (1981) Geochemical evolution of the south mountain batholith, Nova Scotia: rare-earth-element evidence. Can Mineral 19:133–145

Nabelek P, Russ-Nabelek C, Denison J (1992a) The generation and crystallization conditions of the Proterozoic Harney Peak leucogranite, Black Hills, South Dakota, USA: petrologic and geochemical constraints. Contrib Mineral Petrol 110:173–191

Nabelek P, Russ-Nabelek C, Haeussler G (1992b) Stable isotope evidence for the petrogenesis and fluid evolution in the Proterozoic Harney Peak leucogranite, Black Hills, South Dakota. Geochim Cosmochim Acta 56:403–417

Pan YM (1997) Controls on the fractionation of isovalent trace elements in magmatic and aqueous systems: evidence from Y/Ho, Zr/Hf and lanthanide tetrad effect - a discussion of the article by M. Bau (1996). Contrib Mineral Petrol 128:405–408

Pan YM, Breaks FW (1997) Rare-earth elements in fluorapatite, Separation Lake area, Ontario; evidence for S-type granite-rare-element pegmatite linkage. Can Mineral 35:659–671

Paton C, Hergt JM, Phillips D, Woodhead JD, Shee SR (2007a) New insights into the genesis of Indian kimberlites from the Dharwar Craton via in situ Sr isotope analysis of groundmass perovskite. Geology 35:1011−1014

Paton C, Woodhead JD, Hergt JM, Phillips D, Shee S (2007b) Strontium isotope analysis of kimberlitic groundmass perovskite via LA-MC-ICP-MS. Geostand Geoanal Res 31:321−330

Peppard DF, Mason GW, Lewey S (1969). A Tetrad effect in the liquid-liquid extraction ordering of lanthanides (III). J Inorg Nucl Chem 31:2271−2272

Peretyazhko IS, Savina EA (2010a) Fluid and magmatic processes in the formation of the Ary-Bulak ongonite massif (eastern Transbaikalia). Russ Geol Geophys 51:1110−1125

Peretyazhko IS, Savina EA (2010b) Tetrad effects in the rare earth element patterns of granitoid rocks as an indicator of fluoride-silicate liquid immiscibility in magmatic systems. Petrology 18:514−543

Peretyazhko IS, Zagorsky VY, Tsareva EA, Sapozhnikov AN (2007) Immiscibility of calcium fluoride and aluminosilicate melts in ongonite from the Ary-Bulak intrusion, Eastern Transbaikal region. Dokl Earth Sci 413:315−320

Piccoli PM, Candela PA (1994) Apatite in felsic rocks; a model for the estimation of initial halogen concentrations in the Bishop Tuff (Long Valley) and Tuolumne Intrusive Suite (Sierra Nevada Batholith) magmas. Am J Sci 294:92−135

Piccoli PM, Candela PA, Williams TJ (1999) Estimation of aqueous HCl and Cl concentrations in felsic systems. Lithos 46:591−604

Ponader CW, Brown Jr GE (1989) Rare earth elements in silicate systems: II. Interactions of La, Gd and Yb with halogens. Geochim Cosmochim Acta 53:2905−2914

Ramos FC, Wolff JA, Tollstrup DL (2004) Measuring ^{87}Sr/^{86}Sr variations in minerals and groundmass from basalts using LA-MC-ICPMS. Chem Geol 211:135−158

Shannon R (1976) Revised effective ionic radii and systematic studies of interatomic distances in halides and chalcogenides. Acta Crystallographica Section A: Crystal Physics, Diffraction, Theoretical and General Crystallography 32:751−767

Simmons WB, Foord EE, Falster AU (1996) Anatectic origin of granitic pegmatites, western Maine, USA. GAC-MAC Annual Meeting., Winnipeg, Abstracts Programme, pp A87

Simmons WB, Webber KL (2008) Pegmatite genesis: state of the art. Eur J Mineral 20:421−438

Sirbescu MLC, Leatherman MA, Student JJ, Beehr AR (2009) Apatite textures and compositions as records of crystalization processes in the Animik Red Ace pegmatite dike, Wisconsin, USA. Can Mineral 47:725−743

Soares DR, Beurlen H, Barreto SDB, Da Silva MRR, Ferreira CM (2008) Compositonal variation of tourmaline-group minerals in the Borborema pegmatite province, Northeastern Brazil. Can Mineral 46:1097−1116

Sun JF, Yang JH, Wu FY, Li XH, Yang YH, Xie LW, Wilde SA (2010) Magma mixing controlling the origin of the Early Cretaceous Fangshan granitic pluton, North China Craton: *In situ* U-Pb age and Sr-, Nd-, Hf- and O-isotope evidence. Lithos 120:421−438

Takahashi Y, Yoshida H, Sato N, Hama K, Yusa Y, Shimizu H (2002) W- and M-type tetrad effects in REE patterns for water-rock systems in the Tono uranium deposit, central Japan. Chem Geol 184:311−335

Tepper JH, Kuehner SM (1999) Complex zoning in apatite from the Idaho Batholith; a record of magma mixing and intracrystalline trace element diffusion. Am Miner 84:581−595

Tomascak PB, Krogstad EJ, Walker RJ (1998) Sm-Nd isotope systematics and the derivation of granitic pegmatites in southwestern Maine. Can Mineral 36:327−337

Tsuboi M (2005) The use of apatite as a record of initial ^{87}Sr / ^{86}Sr ratios and indicator of magma processes in the Inagawa pluton, Ryoke belt, Japan. Chem Geol 221:157−169

Veksler IV, Dorfman AM, Kamenetsky M, Dulski P, Dingwell DB (2005) Partitioning of lanthanides and Y between immiscible silicate and fluoride melts, fluorite and cryolite and the origin of the lanthanide tetrad effect in igneous rocks. Geochim Cosmochim Acta 69:2847−2860

Von Blackenburg F (1992) Combined high-precision chronometry and geochemical tracing using accessory minerals: applied to the Central-Alpine Bergell intrusion (central Europe). Chem Geol 100:19−40

Wang DH, Chen YC, Xu ZG, Li TD, Fu XJ (2002) The Ore-forming series and law in Altay ore-forming province. Yuanzineng Publish House, Beijing, pp493 (in Chinese)

Wang DH, Cheng YC, Xu ZG (2003) ^{40}Ar/^{39}Ar isotope dating on muscovites from Indosinian rare metal deposits in Central Altay, Northwestern China. Bull Mineral Petrol Geochem 22:14−17 (in Chinese with English abstract)

Wang RC, Che XD, Zhang WL, Zhang AC, Zhang H (2009) Geochemical evolution and late re-equilibration of Na-Cs-rich beryl from the Koktokay# 3 pegmatite (Altai, NW China). Eur J Mineral 21:795−809

Wang RC, Hu H, Zhang AC, Fontan F, Zhang H, Parseval PD (2006a) Occurrence and late re-equilibration of pollucite from the Koktokay no. 3 pegmatite, Altai, northwestern China. Am Miner 91:729−739

Wang RC, Hu H, Zhang AC, Parseval PD, Jiang SY (2007a) Cs-dominant polylithionite in the Koktokay# 3 pegmatite, Altai, NW China: in situ micro-characterization and implication for the storage of radioactive cesium. Contrib Mineral Petrol 153:355−367

Wang T, Hong DW, Jahn BM, Tong Y, Wang YB (2006b) Timing, petrogenesis and setting of Paleozoic syn-orogenic intrusions from the Altai Mountains, NW China: implications for tectonic evolution of an accretionary orogen. J Geol 114:735−751

Wang T, Tong Y, Jahn BM, Zou TR, Wang YB, Hong DW, Han BF (2007b) SHRIMP U-Pb Zircon geochronology of the Altai No. 3 Pegmatite, NW China and its implications for the origin and tectonic setting of the pegmatite. Ore Geol Rev 32:325−336

Wang X, Zhou TR, Xu J, Yu X, Qiu Y (1981) Mineralogy of the pegmatites in Altay. Science Press, Beijing, pp140 (in Chinese)

Webster JD (1990) Partitioning of F between H_2O and CO_2 fluids and topaz rhyolite melt: Implications for mineralizing magmatic-hydrothermal fluids in F-rich granitic systems. Contrib Mineral Petrol 104:424−438

Webster JD (2004) The exsolution of magmatic hydrosaline chloride liquids. Chem Geol 210:33−48

Woodhead J, Swearer S, Hergt J, Maas R (2005) In situ Sr-isotope analysis of carbonates by LA-MC-ICP-MS: interference corrections, high spatial resolution and an example from otolith studies. J Anal At Spectrom 20:22−27

Wu CN, Zhu JC, Liu CS, Yang SZ, Zhu BY, Ning GJ (1995) A study on the inclusions in beryls from Kuwei and Keketuohai pegmatites, Altai, Xinjiang. J Nanjing University 31:351−356 (in Chinese with English abstract)

Wu CZ, Liu SH, Gu LX, Zhang ZZ, Lei RX (2011) Formation mechanism of the lanthanide tetrad effect for a topaz- and amazonite-bearing leucogranite pluton in eastern Xinjiang, NW China. J Asian Earth Sci 42:903−916

Wu FY, Sun DY, Jahn BM, Wilde S (2004) A Jurassic garnet-bearing granitic pluton from NE China showing tetrad REE patterns. J Asian Earth Sci 23:731−744

Yang YH, Sun JF, Xie LW, Fan HR, Wu FY (2008) In situ Nd isotopic measurement of natural geological materials by LA-MC-ICPMS. Chin Sci Bull 53:1062−1070

Yang YH, Wu FY, Wilde SA, Liu XM, Zhang YB, Xie LW, Yang JH (2009) In situ perovskite Sr-Nd isotopic constraints on the petrogenesis of the Ordovician Mengyin kimberlites in the North China Craton. Chem Geol 264:24−42

Yasnygina T, Rasskazov S (2008) Tetrad effect in rare earth element distribution patterns: Evidence from the Paleozoic granitoids of the Oka zone, Eastern Sayan. Geochem Int 46:814−825

Yurimoto H, Duke EF, Papike JJ, Shearer CK (1990) Are discontinuous chondrite-normalized REE patterns in pegmatitic granite systems the results of monazite fractionation? Geochim Cosmochim Acta 54:2141−2145

Zhang AC, Wang RC, Hu H, Chen XM, Zhang H (2004a) Occurrences of foitite and rossmanite from the Koktokay No. 3 granitic pegmatite dyke, Altai, northwestern China: A record of hydrothermal fluids. Can Mineral 42:873−882

Zhang AC, Wang RC, Hu H, Zhang H, Zhu JC, Chen XM (2004b) Chemical evolution of Nb-Ta oxides and zircon from the Koktokay No. 3 granitic pegmatite, Altai, northwestern China. Mineral Mag 68:739−756

Zhang AC, Wang RC, Jiang SY, Hu H, Zhang H (2008a) Chemical and textural features of tourmaline from the spodumene-subtype Koktokay no. 3 pegmatite, Altai, northwestern China: a record of magmatic to hydrothermal evolution. Can Mineral 46:41−58

Zhang AC, Wang RC, Li Y, Hu H, Lu X, Ji J Zhang H (2008b) Tourmalines from the Koktokay No. 3 pegmatite, Altai, NW China: spectroscopic characterization and relationships with the pegmatite evolution. Eur J Mineral 20:143−154

Zhang XH, Mao Q, Zhang HF, Wilde SA (2008c) A Jurassic peraluminous leucogranite from Yiwulushan, western Liaoning, North China craton: age, origin and tectonic significance. Geol Mag 145:305−320

Zhao JX, Cooper JA (1993) Fractionation of monazite in the development of V-shaped REE patterns in leucogranite systems: Evidence from a muscovite leucogranite body in central Australia. Lithos 30:23−32

Zhao ZH, Bao Z, Qiao Y (2010) A peculiar composite M- and W-type REE tetrad effect: Evidence from the Shuiquangou alkaline syenite complex, Hebei Province, China. Chin Sci Bull 55:2684−2696

Zhao ZH, Xiong XL, Han XD, Wang YX, Wang Q, Bao ZW, Jahn BM (2002) Controls on the REE tetrad effect in granites: Evidence from the Qianlishan and Baerzhe Granites, China. Geochem J 36:527−543

Zhu YF, Zeng YS, Gu LB (2006) Geochemistry of the rare metal-bearing pegmatite No. 3 vein and related granites in the Keketuohai region, Altay Mountains, northwest China. J Asian Earth Sci 27:61−77

Zou TR, Li QC (2006) Rare-metal and Rare Earth metal deposits in Xinjiang, China. Geology Press, Beijing, pp34−59 (in Chinese)

Zou TR, Zhang X, Jia F, Wang R (1986) The origin of No. 3 pegmatite in Altayshan, Xinjiang. Miner Depos 5:34−48 (in Chinese with English abstract)

Figure Captions:

Fig. 1 (a) Geological map of the Koktokay region showing the occurrence of the Koktokay No. 3 pegmatite, (b) Vertical sections from A to B and C to D showing the pegmatite, (c) Zonation of the Koktokay No. 3 pegmatite (after Zou et al. 1986), (d) Three-dimensional structure of the Koktokay No. 3 pegmatite showing its internal zonation (after Wang et al. 1981). Sample localities are also shown. The schist includes Ordovician, Devonian and Carboniferous biotite quartz schist, two-mica schist and staurolite-bearing biotite schist

Fig 2 Variations of Mn (wt.%) and XF in apatite

Fig. 3 Variation of (a) Y vs. Sr, (b) LREE vs. HREE, (c) U vs. Th and (d) Th/U vs. Pb in apatite from Koktokay region

Fig. 4 Chondrite-normalized REE patterns of apatite and whole rock samples from Koktokay region. Chondrite REE values from Anders and Grevesse (1989). Red lines represent unpublished whole rock data and data from Liu et al. (2005) and Zou and Li (2006). Blue lines represent apatite data from Liu and Zhang (2005)

Fig. 5 Frequency distribution of the sizes of the tetrad effect T and $TE_{1,3}$ for all analyzed apatite from Koktokay regions

Fig. 6 Variation of $TE_{1,3}$ a parameter illustrating the tetrad effect for apatite versus (a) Y/Ho and (b) F of apatite. The “CHARAC field” with 24<Y/Ho<34 is from Bau (1996)

Fig. 7 Backscattered electron images of apatite each showing one traverse to illustrate the distributions of the major and trace elements including CaO, P_2O_5, MnO, F, Sr, Y, La, Ce and Yb. The spot numbers shown on the backscattered electron images are consistent with the numbers shown in the plots of element variations, each spot representing a single analysis. On the element variation plots the gray line displays the variation of major elements and the dark line the variation of trace elements

Fig. 8 Variations of MnO vs. CaO in apatite

Fig. 9 Variations of (a) Pb, (b) Th, (c) Y, (d) REE, (e) Sr/Y and (f) Y/Ho in apatite

Table Captions:

Table 1 Summary of apatite samples investigated in this study

Table 2 Representative major and trace element compositions of apatite from the Altay Koktokay region

line figure
Click here to download line figure: Fig2.eps

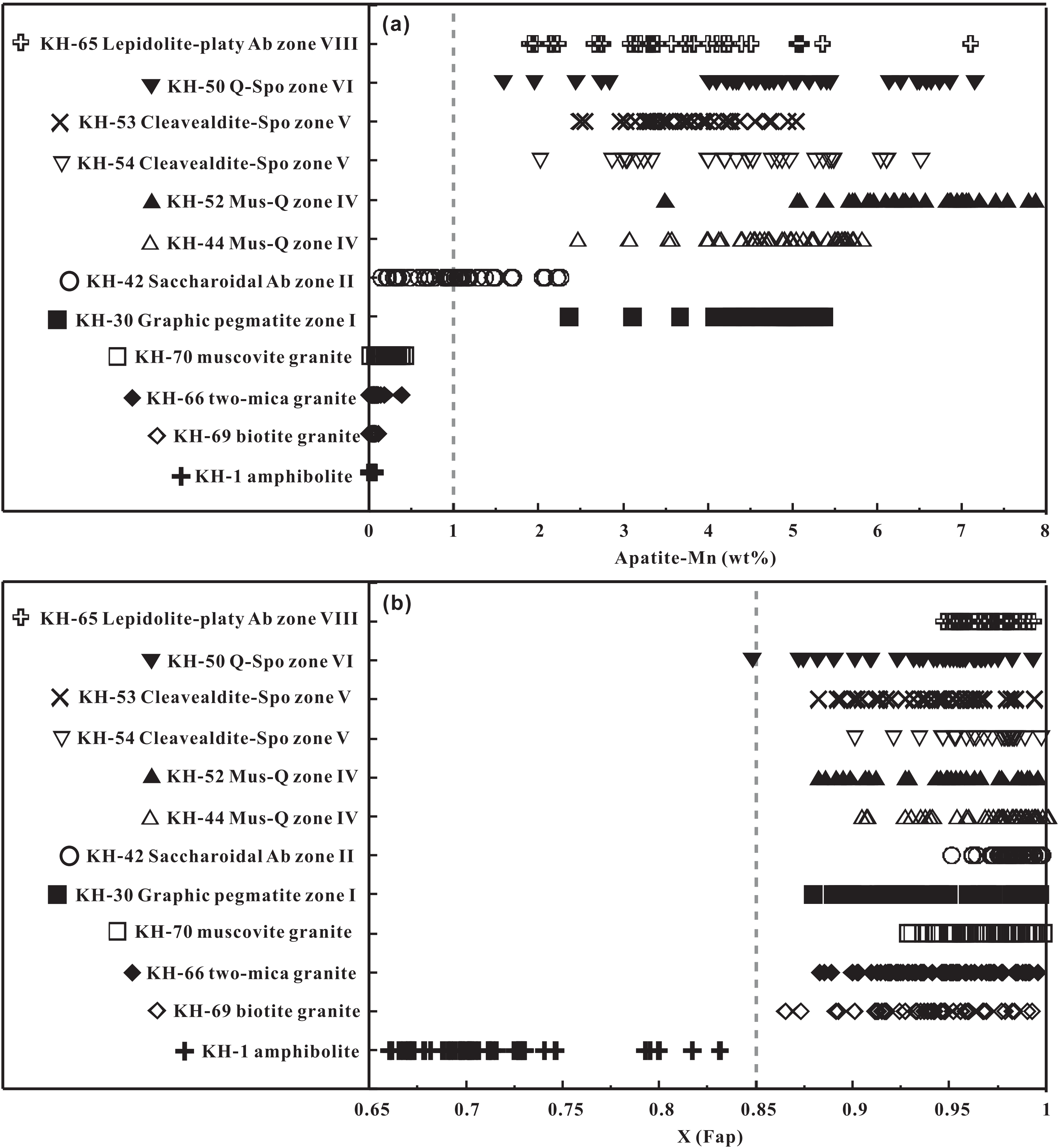

line figure

Click here to download line figure: Fig3.eps

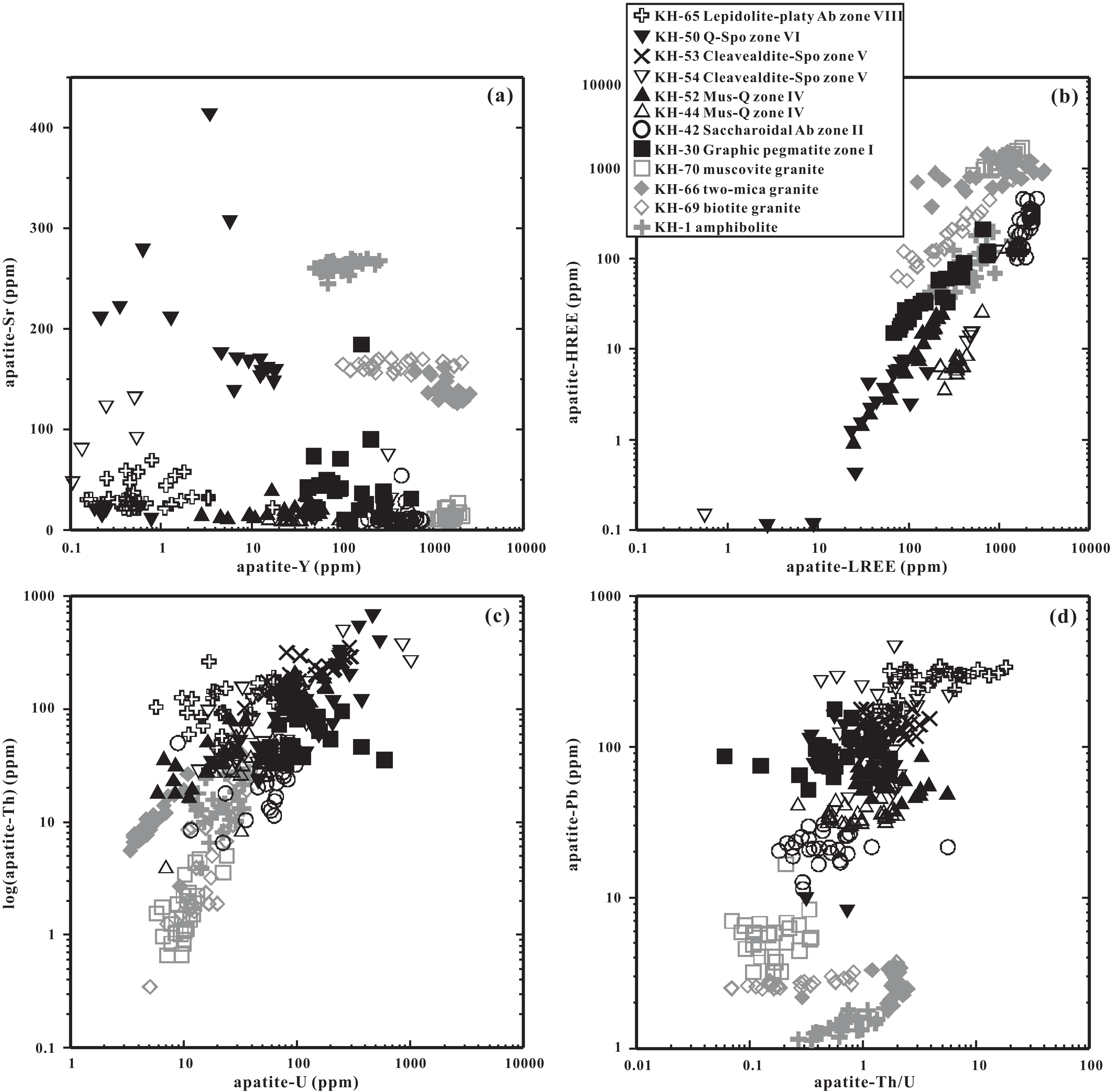

colour figure

Click here to download colour figure: Fig4.eps

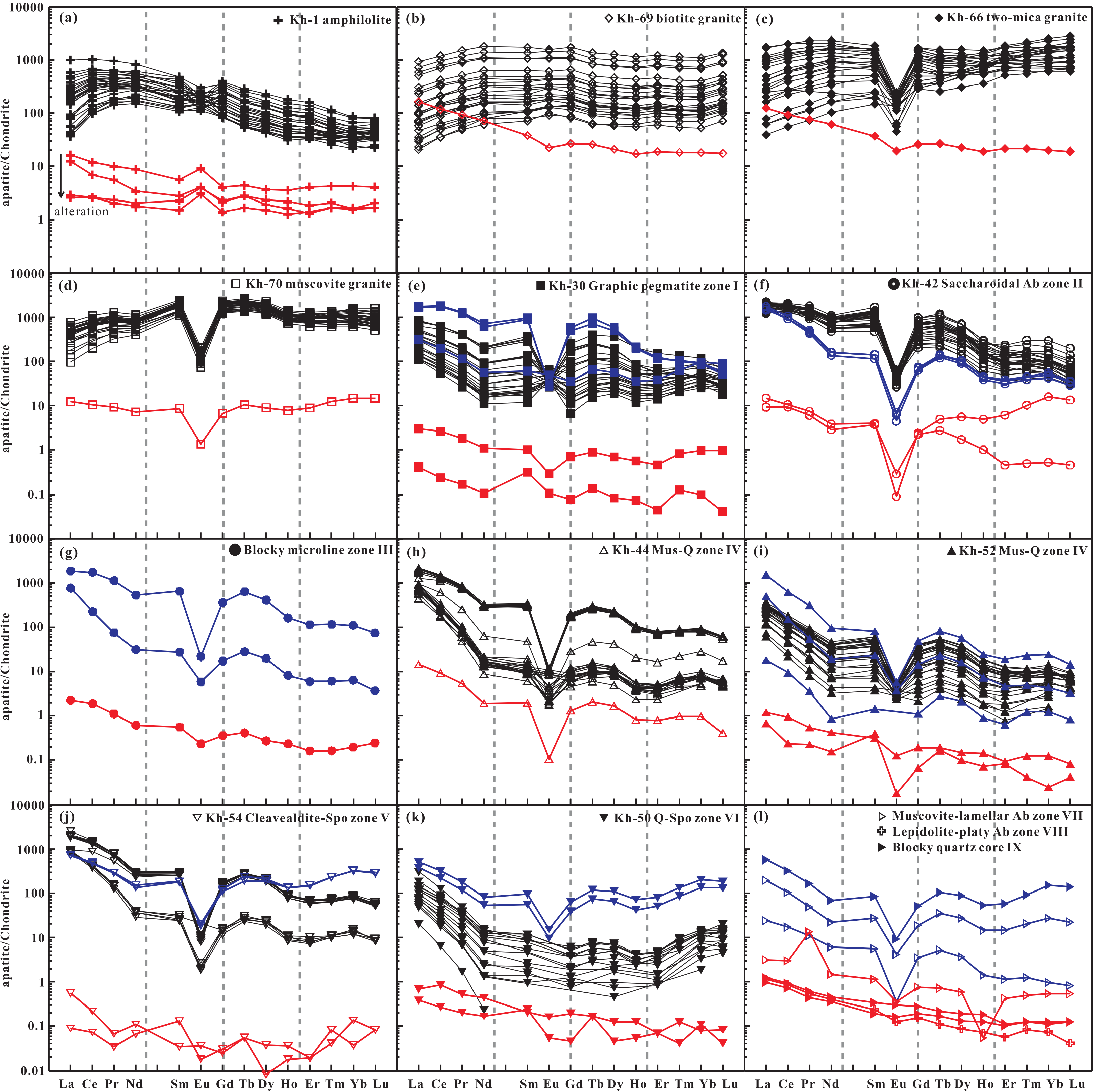

colour figure

Click here to download colour figure: Fig5.eps

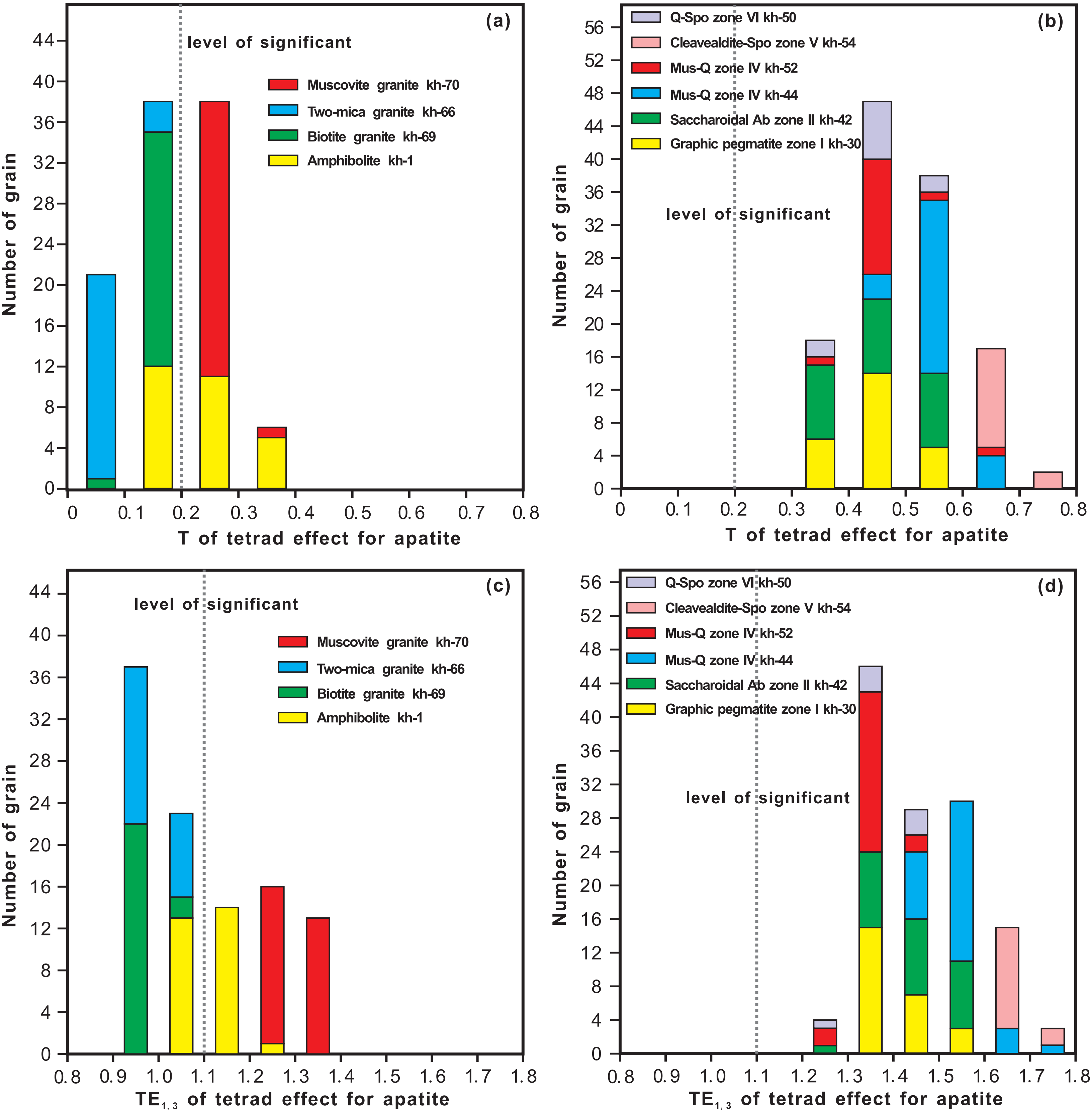

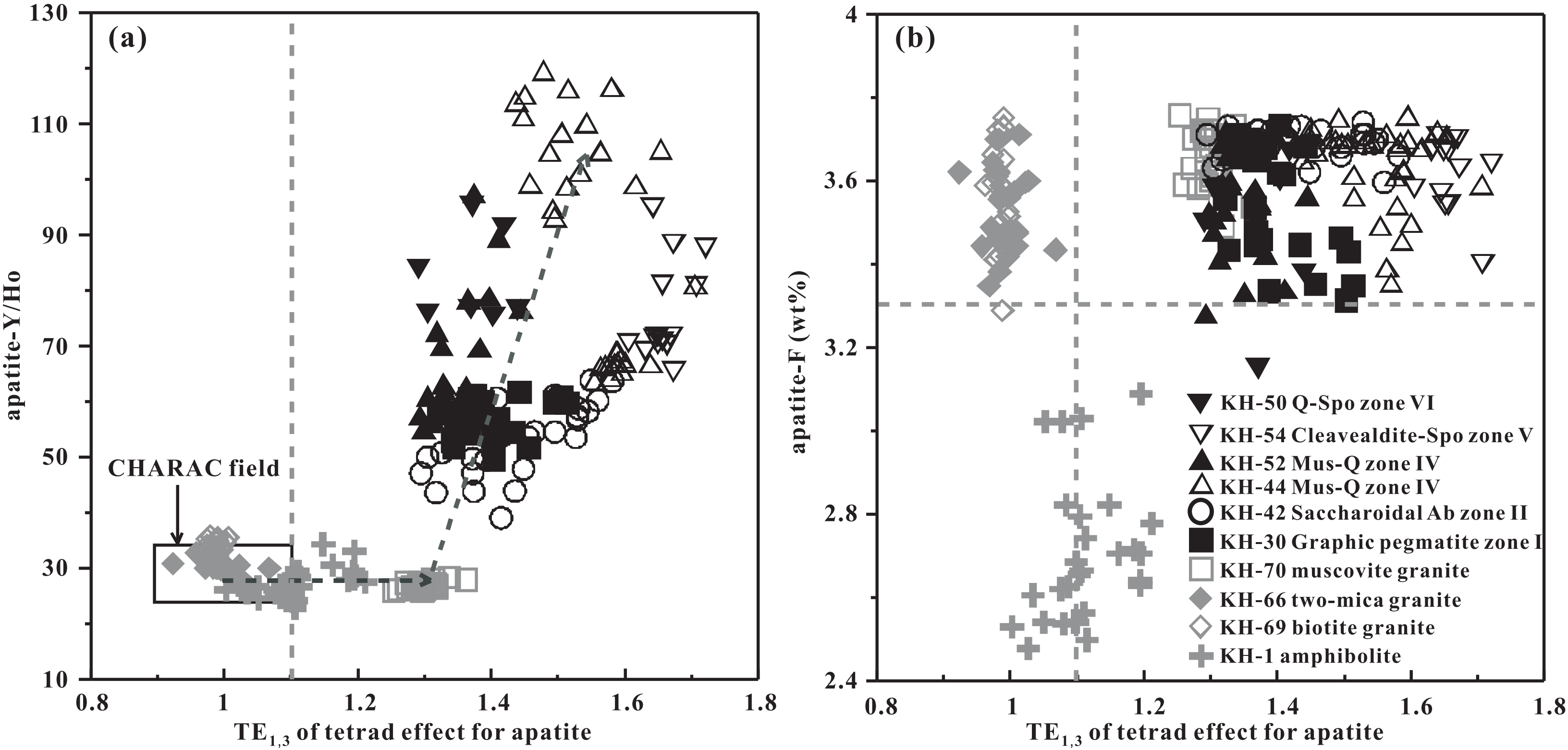
(a)
apatite-Y/Ho
130
110
90
70
50
30
10
CHARAC field
0.8
1
1.2
1.4
1.6
1.8
$TE_{1,3}$ of tetrad effect for apatite
(b)
apatite-F (wt%)
4
3.6
3.2
2.8
2.4
0.8
1
1.2
1.4
1.6
1.8
$TE_{1,3}$ of tetrad effect for apatite
▼ KH-50 Q-Spo zone VI
▽ KH-54 Cleavealdite-Spo zone V
▲ KH-52 Mus-Q zone IV
△ KH-44 Mus-Q zone IV
○ KH-42 Saccharoidal Ab zone II
■ KH-30 Graphic pegmatite zone I
□ KH-70 muscovite granite
◆ KH-66 two-mica granite
◇ KH-69 biotite granite
✚ KH-1 amphibolite

line figure

Click here to download line figure: Fig7.eps

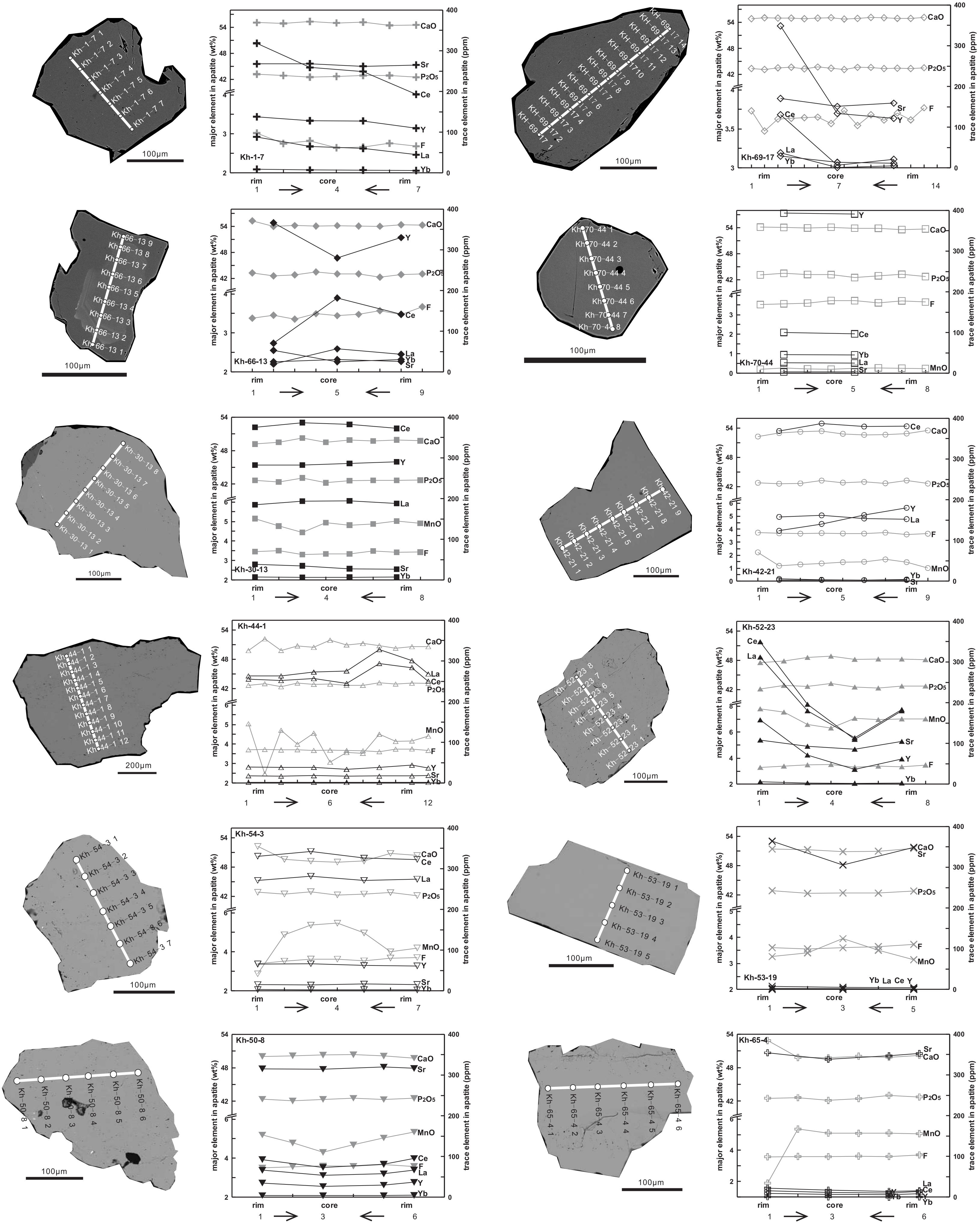

line figure
Click here to download line figure: Fig8.eps

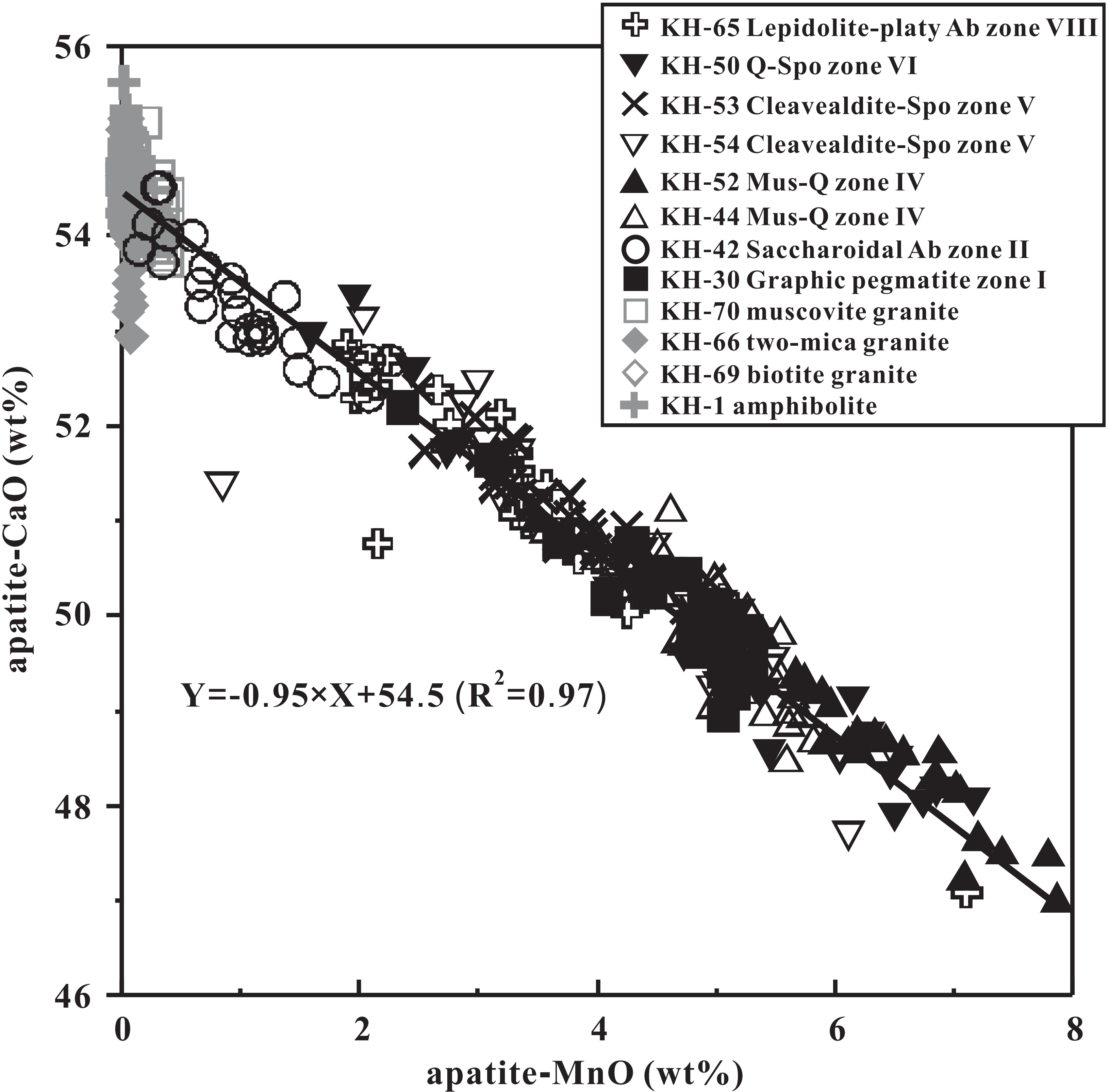

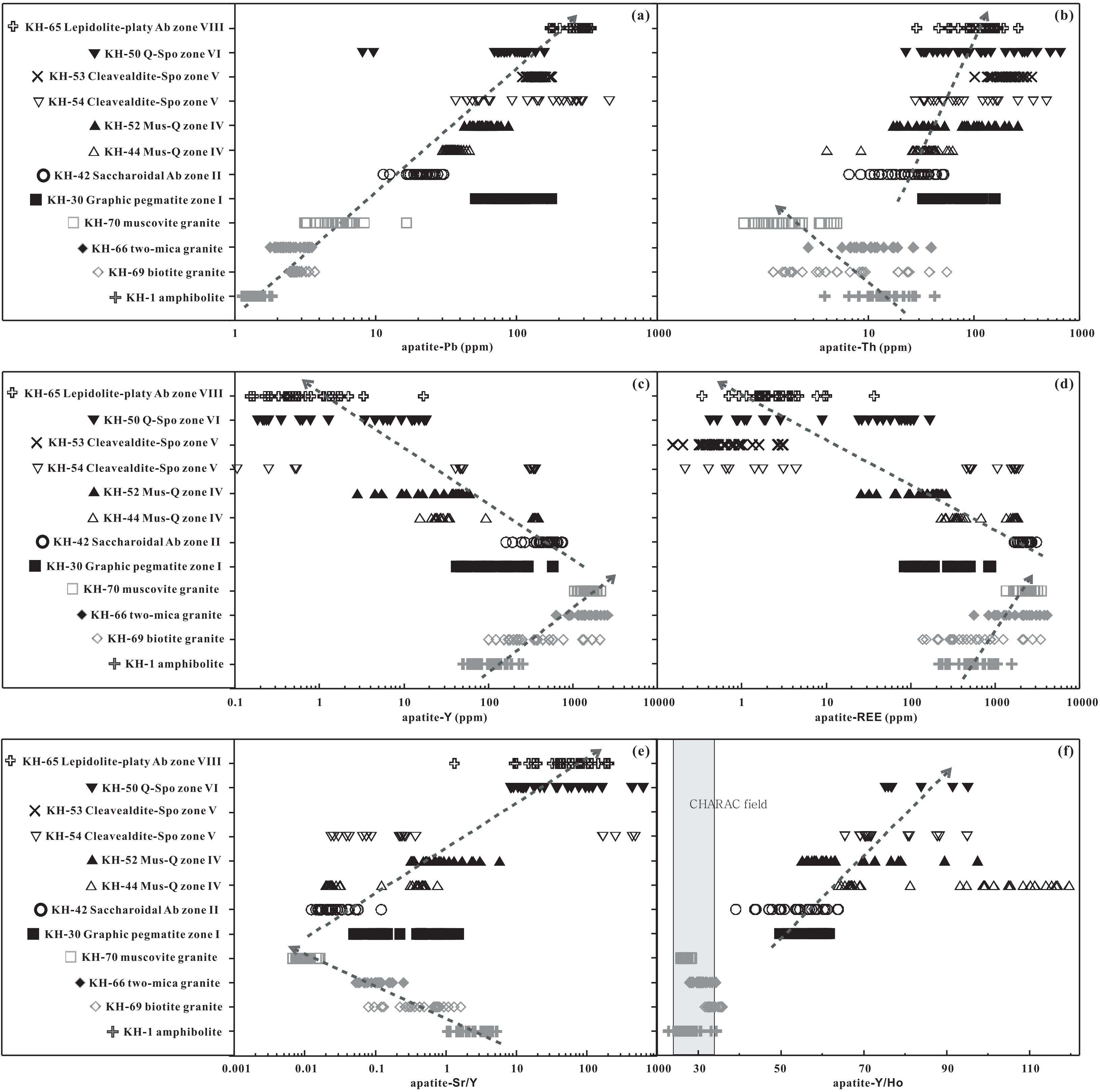
(a)
(b)
(c)
(d)
(e)
(f)
KH-65 Lepidolite-platy Ab zone VIII
KH-50 Q-Spo zone VI
KH-53 Cleavealdite-Spo zone V
KH-54 Cleavealdite-Spo zone V
KH-52 Mus-Q zone IV
KH-44 Mus-Q zone IV
KH-42 Saccharoidal Ab zone II
KH-30 Graphic pegmatite zone I
KH-70 muscovite granite
KH-66 two-mica granite
KH-69 biotite granite
KH-1 amphibolite
1
10
100
1000
apatite-Pb (ppm)
10
100
1000
apatite-Th (ppm)
0.1
1
10
100
1000
10000
apatite-Y (ppm)
1
10
100
1000
10000
apatite-REE (ppm)
0.001
0.01
0.1
1
10
100
1000
apatite-Sr/Y
CHARAC field
30
50
70
90
110
apatite-Y/Ho

Table 1 Summary of apatite samples investigated in this study

Sample	lithology/ pegmatite zone	Mineral assemblage	Major accessory mineral phases	MI in Ap
kh-1	amphibolite	Am (80), Pl (20)	Ap	Am
kh-69	biotite granite	Olg (40-50), Qtz (30-40), Mc (15-20), Bt (5-6)	Ap, Zrc	Zrc, Kfs
kh-66	two-mica granite	Ab (40-45), Qtz (30-35), Mc(15-20), Bt (2-5), Mus (2-5)	Ap, Zrc	
kh-70	muscovite granite	Ab (40-50), Qtz (30-40), Mc (15-20), Mus (5-6)	Ap, Zrc, Grt	
kh-30	graphic pegmatite zone I	Mc (43), Ab (17), Qtz (31), Mus (6)	Ap,Brl, Sps-Alm	
kh-42	saccharoidal albite zone II	Mc (50), Ab (53), Qtz(10), Mus (4)	Ap,Brl, Col-Tan, Sps-Alm	
kh-44	muscovite-quartz zone IV	Mc (21), Ab (8), Qtz (54), Mus (15)	Spd, Ap,Brl, Col-Tan, Srl, Sps-Alm	Mnz
kh-52	muscovite-quartz zone IV	Mc (21), Ab (8), Qtz (54), Mus (15)	Spd, Ap,Brl, Col-Tan, Srl, Sps-Alm	Bsm, Urm
kh-54	cleacelandite-spodumene zone V	Mc (1), Ab (51), Qtz (30), Mus (5), Spd (12)	Ap, Brl, Col-Tan, Urm, Srl, Trp	Col-Tan
kh-53	cleacelandite-spodumene zone V	Mc (1), Ab (51), Qtz (30), Mus (5), Spd (12)	Ap, Brl, Col-Tan, Urm, Srl, Trp	Col-Tan, Zrc
kh-50	quartz-spodumene zone VI	Mc (1), Ab (22), Qtz (55), Mus (4), Spd (17)	Ap, Brl, Col-Tan, Pol, Urm, Trp	Py, Urm
kh-65	lepidolite-albite zone VIII	Mc (1), Ab (31), Qtz (2), Spo (1), Lpd (64)	Ap, Brl, Col-Tan, Pol	

Note: Relative abundances of rock-forming minerals for the first four samples were estimated in vol%, and for pegmatite zones were estimatied in wt% (simplified from Wang et al. 1981 and Zou et al. 1986). Abbreviations: Ab: Albite, Am: Amphibole, Ap: Apatite, Brl: Beryl, Bsm: Bismuthinite, Bt: Biotite, Col-Tan: Columbite-Tantalite series, Grt: garnet, Kfs: K-feldspar, Lpd: Lepidolite, Mc: Microcline, Mnz: Monazite, Mus: Muscovite, Olg: Oligoclase, Pl: Plagioclase, Pol: Pollucite, Py: Pyrite, Qtz: Quartz, Spd: Spodumene, Sps-Alm: Spessartine-Almandine series, Srl: Schorl, Trp: Triplite, Urm: Uramicrolite, Zrc: Zircon. MI: Mineral Inclusion

Table 2 Representative major and trace element compositions of apatite from the Koktuokay region

Lithology/ pegmatite zone	plagioclase amphibolite		biotite granite		biotite-muscovite granite		muscovite granite	
sample	kh-1		Kh-69		kh-66		kh-70	
			Major element					
n	41	σ	48	σ	78	σ	51	σ
P_2O_5 (wt%)	43.00	*0.40*	43.06	*0.39*	42.36	*1.21*	42.98	*0.31*
CaO	54.73	*0.37*	54.85	*0.24*	54.03	*1.06*	54.23	*0.34*
SiO_2	–		–		–		–	
Al_2O_3	–		–		–		–	
FeO	0.02	*0.03*	0.02	*0.02*	0.03	*0.09*	0.03	*0.02*
MnO	0.03	*0.02*	0.05	*0.02*	0.07	*0.05*	0.24	*0.09*
Na_2O	–		–		–		–	
Cl	–		–		–		–	
F	2.70	*0.17*	3.57	*0.12*	3.55	*0.11*	3.66	*0.07*
sum	100.48		101.55		100.04		101.14	
F =-O	-0.95		-0.20		-0.18		-0.10	
Total	99.53		101.35		99.86		101.04	
			Cations on the basis of 3 P apfu					
P (apfu)	3.037		3.033		3.023		3.045	
Ca	4.892		4.890		4.881		4.862	
Mn	0.002		0.003		0.005		0.017	
F	0.713		0.940		0.946		0.968	
X(Fap)	0.71		0.94		0.95		0.97	
X(Hap)	0.29		0.06		0.05		0.03	
			Trace elements					
n	28		24		23		28	
V (ppm)	8.33	*4.39*	8.78	*8.11*	5.56	*4.46*	–	
Sr	262.7	*5.58*	163.7	*4.69*	140.6	*10.15*	14.57	*4.49*
Y	106.5	*52.41*	527.3	*533.1*	1452	*479.7*	1490	*251.8*
La	54.83	*48.24*	47.35	*57.20*	131.7	*118.0*	98.93	*36.42*
Ce	209.7	*126.3*	167.0	*191.4*	434.0	*357.3*	385.4	*119.0*
Pr	34.14	*16.38*	30.94	*35.42*	74.77	*58.09*	70.16	*18.39*
Nd	167.5	*70.49*	189.2	*211.2*	428.5	*303.4*	344.2	*71.42*
Sm	35.24	*15.76*	60.62	*65.78*	129.5	*78.51*	258.2	*47.59*
Eu	10.46	*2.58*	24.23	*24.27*	8.94	*3.00*	7.70	*1.64*
Gd	36.04	*18.49*	84.79	*88.36*	181.2	*90.05*	354.2	*57.88*
Tb	4.38	*2.34*	12.03	*12.66*	28.91	*12.88*	70.73	*11.76*
Dy	23.16	*12.31*	74.60	*77.79*	203.0	*77.43*	400.3	*63.31*
Ho	4.01	*2.11*	15.97	*16.49*	47.70	*15.75*	55.23	*8.79*
Er	10.52	*5.16*	49.45	*50.73*	169.1	*56.01*	142.4	*24.38*
Tm	1.22	*0.53*	7.01	*7.20*	27.85	*10.43*	22.05	*4.55*
Yb	6.87	*2.50*	46.36	*47.72*	208.6	*86.47*	161.6	*40.19*
Lu	1.07	*0.35*	8.94	*9.04*	33.21	*14.73*	21.56	*6.21*
Pb	1.43	*0.20*	2.77	*0.30*	2.55	*0.54*	5.64	*2.51*
Th	16.28	*8.12*	9.92	*13.33*	12.00	*7.86*	1.89	*1.22*
U	23.90	*10.16*	18.02	*8.46*	7.01	*6.01*	10.73	*4.05*
sum REE	599.1		818.5		2107		2393	
Y/Ho	27.22		33.58		30.48		26.95	
Th/U	0.72		0.45		1.83		0.17	
Eu/Eu*	1.07		1.08		0.25		0.19	
$(La/Yb)_N$	5.21		0.60		0.65		1.71	
T	0.22	*0.07*	0.12	*0.01*	0.08	*0.04*	0.25	*0.03*
$TE_{1,3}$	1.11	*0.06*	0.99	*0.01*	0.99	*0.05*	1.29	*0.06*

Table 2 continued

Lithology/ pegmatite zone	Graphic pegmatite zone I		Saccharoidal Ab zone II		Mus-Q zone IV			
sample	kh-30		kh-42		kh-44		kh-52	
Major element								
n	41	σ	45	σ	41	σ	30	σ
P_2O_5 (wt%)	42.56	*0.22*	42.72	*0.33*	42.59	*0.37*	42.50	*0.34*
CaO	49.92	*0.65*	53.31	*0.58*	49.89	*1.00*	48.64	*0.85*
SiO_2	–		–		–		–	
Al_2O_3	–		–		–		–	
FeO	0.13	*0.05*	0.03	*0.02*	0.12	*0.06*	0.13	*0.06*
MnO	4.77	*0.59*	1.04	*0.55*	4.87	*0.88*	6.39	*0.93*
Na_2O	–		–		–		–	
Cl	–		–		–		–	
F	3.53	*0.14*	3.69	*0.04*	3.62	*0.13*	3.53	*0.13*
sum	100.91		100.79		101.09		101.19	
F=-O	-0.18		-0.06		-0.10		-0.18	
Total	100.73		100.73		100.99		101.01	
Cations on the basis of 3 P apfu								
P (apfu)	3.048		3.045		3.048		3.047	
Ca	4.525		4.808		4.518		4.413	
Fe	0.009		0.002		0.008		0.010	
Mn	0.342		0.074		0.349		0.458	
F	0.945		0.982		0.968		0.946	
X(Fap)	0.95		0.98		0.97		0.95	
X(Hap)	0.05		0.02		0.03		0.05	
Trace elements								
n	25		27		31		26	
V (ppm)	–		–		–		–	
Sr	42.58	*35.42*	12.52	*9.23*	10.18	*1.47*	20.18	*7.13*
Y	154.8	*122.2*	467.0	*149.3*	170.0	*168.7*	30.08	*17.14*
La	83.17	*58.53*	423.3	*60.55*	286.3	*148.8*	53.01	*21.54*
Ce	148.1	*124.2*	999.7	*134.5*	443.1	*337.2*	63.44	*29.71*
Pr	13.59	*12.47*	119.5	*19.25*	34.52	*32.08*	4.71	*2.45*
Nd	32.82	*32.15*	357.2	*69.90*	62.84	*65.34*	10.72	*6.16*
Sm	15.43	*16.67*	150.9	*46.13*	20.61	*22.42*	4.40	*2.74*
Eu	2.28	*0.61*	2.59	*0.68*	0.39	*0.22*	0.23	*0.06*
Gd	13.00	*14.17*	106.7	*41.75*	16.32	*17.44*	3.89	*2.57*
Tb	3.64	*3.79*	22.55	*9.35*	4.51	*4.87*	1.02	*0.60*
Dy	21.63	*20.19*	95.27	*37.99*	23.98	*25.45*	4.69	*2.96*
Ho	2.72	*2.27*	9.07	*3.62*	2.46	*2.61*	0.54	*0.28*
Er	6.39	*4.46*	17.43	*7.68*	5.35	*5.52*	1.02	*0.61*
Tm	1.11	*0.58*	2.77	*1.37*	1.01	*0.95*	0.19	*0.06*
Yb	8.21	*3.51*	16.51	*8.74*	6.82	*6.51*	1.15	*0.60*
Lu	0.88	*0.37*	1.55	*0.90*	0.76	*0.67*	0.16	*0.04*
Pb	92.45	*29.37*	21.62	*4.49*	35.88	*4.15*	60.06	*10.46*
Th	70.97	*38.50*	26.05	*12.52*	35.85	*11.86*	86.47	*66.76*
U	133.8	*117.9*	57.03	*23.48*	39.71	*17.75*	66.36	*66.30*
sum REE	353.0		2325		908.8		148.9	
Y/Ho	57.17		53.26		89.10		66.20	
Th/U	0.72		0.65		1.05		1.95	
Eu/Eu*	2.20		0.07		0.13		0.17	
$(La/Yb)_N$	7.42		21.16		65.21		35.07	
T	0.44	*0.05*	0.45	*0.08*	0.56	*0.05*	0.45	*0.05*
$TE_{1,3}$	1.34	*0.28*	1.44	*0.09*	1.55	*0.06*	1.35	*0.04*

Table 2 continued

Lithology/ pegmatite zone	Cleavealbite-Spo zone V				Q-Spo zone VI		Thin sliced Ab- Lep zone VIII	
sample	kh-54		kh-53		kh-50		kh-65	
			Major element					
n	28	σ	34	σ	35	σ	34	σ
P_2O_5 (wt%)	42.49	*0.59*	42.61	*0.28*	42.23	*0.39*	42.59	*0.42*
CaO	50.30	*1.32*	51.00	*0.61*	49.91	*1.42*	51.09	*1.14*
SiO_2	–		–		–		–	
Al_2O_3	–		–		–		–	
FeO	0.06	*0.06*	0.03	*0.02*	0.07	*0.04*	0.03	*0.03*
MnO	4.35	*1.33*	3.80	*0.67*	4.90	*1.43*	3.61	*1.15*
Na_2O	–		–		–		–	
Cl	–		–		–		–	
F	3.59	*0.16*	3.52	*0.11*	3.50	*0.14*	3.62	*0.06*
sum	100.79		100.96		100.61		100.94	
F=-O	-0.12		-0.20		-0.17		-0.11	
Total	100.67		100.76		100.44		100.83	
			Cations on the basis of 3 P apfu					
P (apfu)	3.046		3.045		3.038		3.045	
Ca	4.563		4.612		4.543		4.622	
Fe	0.004		0.002		0.005		0.002	
Mn	0.312		0.271		0.353		0.258	
F	0.961		0.941		0.940		0.968	
X(Fap)	0.96		0.94		0.95		0.97	
X(Hap)	0.04		0.06		0.05		0.03	
			Trace elements					
n	24		30		27		30	
V (ppm)	–		–		–		–	
Sr	42.40	*38.58*	21.89	*3.16*	203.0	*248.5*	35.18	*13.52*
Y	169.0	*159.2*	–		6.67	*6.58*	1.42	*3.05*
La	219.5	*210.3*	0.78	*0.66*	16.14	*17.39*	1.96	*2.92*
Ce	388.7	*381.4*	0.33	*0.31*	19.58	*21.65*	1.81	*3.16*
Pr	43.81	*28.62*	–		1.97	*1.31*	–	
Nd	86.16	*54.63*	–		3.02	*2.44*	0.32	*0.51*
Sm	28.14	*18.80*	–		0.81	*0.58*	0.17	*0.16*
Eu	0.42	*0.21*	–		–		–	
Gd	19.58	*14.70*	–		0.57	*0.37*	–	
Tb	6.40	*4.24*	–		0.20	*0.07*	–	
Dy	32.95	*21.47*	–		0.90	*0.57*	–	
Ho	3.23	*2.09*	–		0.19	*0.04*	–	
Er	7.16	*4.56*	–		0.46	*0.24*	–	
Tm	1.18	*0.72*	–		0.19	*0.04*	–	
Yb	9.31	*5.57*	–		1.49	*0.77*	–	
Lu	0.96	*0.58*	–		0.28	*0.11*	–	
Pb	227.4	*296.1*	144.0	*18.92*	95.32	*32.41*	274.3	*53.01*
Th	112.1	*112.6*	210.2	*59.01*	160.2	*160.2*	121.4	*47.14*
U	130.5	*253.4*	145.5	*79.18*	171.0	*138.4*	38.54	*29.43*
sum REE	708.9		1.07		40.17		4.05	
Y/Ho	75.93		–		82.09		–	
Th/U	1.80		1.77		1.01		5.13	
Eu/Eu*	0.06		−		−		−	
$(La/Yb)_N$	38.60		−		−		−	
T	0.65	*0.05*	−		0.44	*0.05*	−	
$TE_{1,3}$	1.66	*0.03*	−		1.37	*0.06*	−	

Major elements wt%, trace elements ppm; − below detection limit; a dash indicates that the value could not be calculated. The normalization is based on the C1 chondrite data given by Anders and Grevesse (1989). The Eu anomaly is defined as $Eu/Eu^* = Eu_N/\sqrt{Sm_N \times Gd_N}$. Tetrad effect is defined as $T = \sqrt{\frac{1}{2N} \times \sum_{i=1}^{N} ([\frac{X_{Bi}}{X_{Ai}^{2/3} \times X_{Di}^{1/3}} - 1]^2 + [\frac{X_{Ci}}{X_{Ai}^{1/3} \times X_{Di}^{2/3}}]^2)}$ (N=1, 3, 4) after Monecke et al. (2002), where X_{Ai}, X_{Bi}, X_{Ci} and X_{Di} are the chondrite-normalized concentrations of the first, second, third and fourth element in tetrad i; and

$$TE_{1,3} = \sqrt{\sqrt{Ce_N / (La_N^{2/3} \times Nd_N^{1/3}) \times \mathrm{Pr}_N / (La_N^{1/3} \times Nd_N^{2/3})} \times \sqrt{Tb_N / (Gd_N^{2/3} \times Ho_N^{1/3}) \times Dy_N / (Gd_N^{1/3} \times Ho_N^{2/3})}}$$

after Irber (1999)

Supplementary spreadsheet 1 LA-ICP-MS analytical results for international reference materials

Element	Mass	NIST SRM 610					BCR-2G				
		This work average (ppm)	SD[†] (ppm)	n	Literature values[a]	Accuracy [‡] (%)	This work average (ppm)	SD[†] ppm)	n	Literature values[a]	Accuracy[‡] (%)
V	51	428	2.98	67	442	-3.3	420.81	5.04	30	425.00	-0.99
Sr	88	520	2.84	67	516	0.8	340.82	3.15	30	342.00	-0.35
Y	89	494	12.4	67	450	9.8	34.75	0.89	30	35.00	-0.71
La	139	448	3.72	67	457	-2.0	24.95	0.37	30	24.70	1.02
Ce	140	461	4.24	67	448	2.9	52.94	0.76	30	53.30	-0.67
Pr	141	455	9.27	67	430	5.9	6.67	0.19	30	6.70	-0.42
Nd	143	447	6.63	67	431	3.8	28.61	0.93	30	28.90	-1.02
Sm	147	466	10.1	67	451	3.3	6.56	0.33	30	6.59	-0.47
Eu	151	466	9.70	67	461	1.0	1.95	0.10	30	1.97	-0.89
Gd	155	469	14.6	67	444	5.6	6.65	0.36	30	6.71	-0.82
Tb	159	459	11.7	67	443	3.7	1.01	0.05	30	1.02	-0.64
Dy	163	453	12.9	67	427	6.1	6.36	0.22	30	6.44	-1.21
Ho	165	457	15.3	67	449	1.9	1.26	0.06	30	1.27	-0.76
Er	166	461	12.2	67	426	8.2	3.60	0.20	30	3.70	-2.57
Tm	169	446	16.8	67	420	6.3	0.51	0.03	30	0.51	0.41
Yb	173	462	19.6	67	445	3.8	3.34	0.28	30	3.39	-1.57
Lu	175	448	11.3	67	435	3.1	0.49	0.04	30	0.50	-2.78
Pb	208	422	8.26	67	426	-1.0	10.81	0.38	30	11.00	-1.71
Th	232	465	9.65	67	457	1.7	5.90	0.17	30	5.90	-0.03
U	238	447	10.8	67	462	-3.0	1.70	0.06	30	1.69	0.46

[†] SD: standard deviation.

‡ Accuray = 100% x [(analytical value/reference value)-1].

Literature values[a] are from GeoReM database (http://georem.mpch-mainz.gwdg.de/)

BHVO-2G					BIR-1G				
This work average (ppm)	SD[†] (ppm)	n	Literature values[a]	Accuracy [‡] (%)	This work average (ppm)	SD[†] (ppm)	n	Literature values[a]	Accuracy [‡] (%)
319	3.75	30	308	3.7	327	6.04	30	326	0.4
397	3.71	30	396	0.3	109	1.51	30	109	0.4
24.5	0.77	30	26.0	-5.7	14.7	0.38	30	14.3	2.6
15.0	0.27	30	15.2	-1.2	0.59	0.04	30	0.61	-2.6
37.7	0.65	30	37.6	0.2	1.92	0.07	30	1.89	1.5
5.21	0.19	30	5.35	-2.7	0.36	0.04	30	0.37	-1.8
24.4	0.77	30	24.5	-0.4	2.41	0.30	30	2.37	1.6
5.98	0.28	30	6.10	-1.9	1.09	0.13	30	1.09	-0.2
2.06	0.10	30	2.07	-0.4	0.53	0.06	30	0.52	1.6
6.01	0.34	30	6.16	-2.4	1.76	0.22	30	1.85	-4.7
0.89	0.05	30	0.92	-3.3	0.34	0.03	30	0.35	-2.1
5.12	0.25	30	5.28	-3.0	2.48	0.20	30	2.55	-2.7
0.93	0.05	30	0.98	-5.4	0.55	0.05	30	0.56	-2.2
2.42	0.12	30	2.56	-5.4	1.67	0.14	30	1.70	-2.0
0.31	0.03	30	0.34	-9.0	0.23	0.02	30	0.24	-2.3
1.89	0.19	30	2.01	-6.0	1.63	0.19	30	1.64	-0.6
0.26	0.03	30	0.28	-6.8	0.24	0.03	30	0.25	-4.0
1.82	0.09	30	1.70	7.3	3.84	0.24	30	3.70	3.8
1.20	0.08	30	1.22	-1.9	0.03	0.02	30	0.03	1.0
0.42	0.04	30	0.40	5.0	0.05	0.03	30	0.02	98.0

Supplementary material Major and trace element compositions of whole rocks from Koktokay region

Lithology/ Zone	Amphibo -lite	biotite-muscovite granite	biotite granite	muscovite granite	zone I	zone II	zone IV	zone IV	zone V	zone V	zone VI	zone VIII
sample	KH-1	KH-66	KH-69	KH-70	KH-30	KH-42	KH-44	KH-52	KH-54	KH-53	KH-50	KH-65
SiO_2 (wt%)	44.36	71.04	68.66	76.34	73.41	72.67	79.05	91.86	78.99	69.45	81.52	69.88
TiO_2	0.92	0.42	0.63	0.022	<0.004	0.007	0.006	0.006	<0.004	<0.004	0.004	<0.004
Al_2O_3	16.63	13.21	13.19	12.56	13.26	15.1	10.1	4.62	13.88	18.69	12.27	17.81
T(Fe_2O_3)	16.08	3.99	4.96	0.71	0.09	1.08	0.69	0.49	0.19	0.20	0.33	0.13
MnO	0.20	0.07	0.08	0.05	0.01	0.71	0.13	0.05	0.06	0.05	0.06	0.08
MgO	7.75	1.05	1.82	0.11	0.04	0.18	0.02	<0.01	0.01	0.02	0.06	<0.01
CaO	9.98	3.09	3.98	0.59	0.13	0.53	0.52	0.13	0.14	0.22	0.16	0.16
Na_2O	0.94	3.86	3.10	3.58	2.75	7.99	3.48	0.86	5.20	10.32	3.92	7.66
K_2O	0.16	2.32	2.66	5.20	9.75	0.99	1.32	1.14	0.95	0.39	0.82	2.50
P_2O_5	0.08	0.11	0.15	0.07	0.12	0.17	0.36	0.07	0.10	0.12	0.05	0.13
LOI	2.67	0.76	0.68	0.71	0.38	0.52	1.08	0.72	0.46	0.47	0.74	1.53
Sum	99.77	99.92	99.91	99.94	99.94	99.95	96.75	99.94	99.97	99.93	99.92	99.88
V (ppm)	481	51.6	88.4	1.1	0.444	0.721	1.19	0.771	0.454	0.316	1.86	0.216
Ga	21.5	18.3	18.8	17.5	14.6	29.2	25.8	15.3	35.3	34.8	30.7	43.6
Rb	5.1	87.9	106	169	954	148	353	389	506	131	370	2618
Sr	185	213	218	11.7	4.04	3.53	4.25	0.401	1.16	1.64	4.66	1.11
Y	5.65	31.5	28	12.1	0.185	11.9	2.96	0.164	0.035	0.04	0.076	0.033
Nb	1.25	7.99	8.27	7.23	1.35	14.4	31.1	86.7	32.9	25.2	50.6	40.4
Cs	2.24	4.23	6.67	3.68	265	7.42	433	49.8	199	66.6	109	1057
Ba	34.7	322	475	12.6	4.83	0.455	4.02	0.434	0.348	0.705	1.5	0.578
La	3.83	29	38	2.89	0.097	3.5	3.43	0.162	0.021	0.025	0.089	0.015
Ce	7.19	57	71	6.28	0.14	6.38	5.67	0.143	0.044	0.051	0.163	0.027
Pr	0.893	6.78	8.34	0.824	0.015	0.657	0.485	0.02	0.003	0.006	0.018	0.002
Nd	3.97	27.8	32.1	3.26	0.048	1.74	0.87	0.07	0.03	0.019	0.076	0.007
Sm	0.82	5.43	5.57	1.26	0.047	0.581	0.287	0.058	0.019	0.002	0.035	0.032
Eu	0.504	1.09	1.27	0.076	0.006	0.005	0.006	0.001	0.001	0.001	0.003	0.001
Gd	0.797	5.07	5.22	1.32	0.015	0.473	0.26	0.013	0.006	0.005	0.009	0.001
Tb	0.158	0.961	0.936	0.375	0.005	0.18	0.076	0.006	0.002	0.003	0.006	0.001
Dy	0.882	5.4	5.04	2.18	0.02	1.35	0.409	0.024	0.002	0.001	0.011	0.001
Ho	0.198	1.07	0.964	0.433	0.004	0.276	0.045	0.004	0.001	0.001	0.003	0.001
Er	0.642	3.41	3	1.39	0.007	0.988	0.127	0.013	0.003	0.004	0.011	0.002
Tm	0.103	0.53	0.449	0.298	0.003	0.249	0.024	0.001	0.001	0.001	0.001	0.001
Yb	0.685	3.29	2.96	2.42	0.016	2.56	0.161	0.004	0.022	0.003	0.018	0.104
Lu	0.098	0.468	0.422	0.361	0.001	0.325	0.01	0.001	0.002	0.001	0.001	0.003
Ta	0.103	0.706	0.649	0.448	0.94	13.7	9.3	27.1	40.5	37.4	270	120
Pb	2.73	12.1	12.1	30.4	39.5	13	13.9	1.97	10.1	13.8	4.58	16.3
Bi	0.83	0.09	0.272	0.277	7.21	6.13	50.2	32.1	3.18	3.44	0.139	2.32
Th	0.632	11.6	10.3	2.46	0.11	9.4	2.32	1.13	2.04	4.15	2.11	3.16
U	0.203	1.98	1.64	0.838	1.04	3.05	4.46	0.581	3.76	1.63	10.4	9.83
Zr	5.22	45	25.3	24.2	7.04	34.5	47.6	1.02	23.5	2.2	12	114
Hf	0.173	1.57	0.858	1.82	0.423	2.13	4.06	0.132	3.44	0.311	2.44	18.4